A Quantitative Exploration of Tension Sensing at Metaphase in Budding Yeast

A DISSERTATION SUBMITTED TO THE FACULTY OF THE GRADUATE SCHOOL

OF THE UNIVERSITY OF MINNESOTA

BY

Soumya Mukherjee

IN PARTIAL FULFILLMENT OF THE REQUIREMENTS FOR THE DEGREE OF

DOCTOR OF PHILOSOPHY

Melissa K. Gardner, Advisor

July, 2018

ACKNOWLEDGEMENTS

I am extremely grateful to my adviser, Melissa Gardner. Working with her over the last few years has been an absolute pleasure. I have had a lot of freedom to pursue my own ideas, as well as a lot of guidance to ensure everything came together into one coherent story. I understand it is a hard balance for an adviser to strike, and I really appreciate all of Melissa's efforts in guiding me this far.

Thank you to Jeremy Chacon for his early work in developing the chromatin stiffness assay and his diligence in addressing concerns from all sides. This work would not have been possible without him. I would like to thank Damien Tank, for his tireless efforts to supply me with a steady stream of yeast strains to image, even if they were ridiculous requests like a double tagged, triple conditional mutant strain. A big big thank you to Mark McClellan for keeping the Gardner lab going, everything would grind to a halt without him. I would also like to thank him for his help with protein purification and Western blot analysis for this project. I'd like to thank Lauren Harasymiw for all of her statistical work, and for a number of enlightening and intellectually stimulating discussions about the nature of tension sensing in the cell. I would also like to thank Qing Yang for his efforts working alongside me on some experiments. A big thank you to members of the Gardner, present and past , especially Courtney Coombes, Taylor Reid and Rebecca Goldblum for helping make the Gardner lab a properly wonderful place to work.

I'd like to thank our collaborators. We had an especially close collaboration with the Duncan Clarke lab, led by his former postdoc Heather Edgerton. This was an extremely fruitful collaboration, yielding a number of papers, as well as insightful ponderances into the almost imponderable mysteries of the Spindle Assembly Checkpoint. I would like to thank Laurie Parker

and her former staff scientist Brian Sandri for their expertise with Mass Spectrometry. I'd also like to thank Judy Berman and her former postdoc, Laura Burrack. Work done with them in *Candida albicans* yielded some useful insights into tension generation and sensing.

I would like to acknowledge all members of the Clarke, Courtemanche and Titus labs for all their insight during lab meetings. I'd like to thank my committee members, Duncan Clarke, Alex Sobeck, Naoko Shima, Mary Porter and Dave Odde for their time and effort.

A big thank you to all my fellow MCSB graduate students, grad school turned into the best years of my life so far largely because of them. Go Mountain Beavers.

Lastly, I must acknowledge the people who led me to take up the study of biology, and to learn to love research. Respectively, they are Manjuli Mukherjee and Shashikant Acharya. None of this would have been possible without their inspiration.

ABSTRACT

During mitosis, motors associate with microtubules to exert forces that push spindle poles apart, thus establishing a mitotic spindle. These pushing forces in turn cause tension in the chromatin that connects oppositely attached sister chromosomes. This tension has been hypothesized to act as a mechanical signal that allows the cell to detect chromosome attachment errors during mitosis. However, the magnitude of changes in tension that could be detected by the cell to initiate an error correction response during metaphase has not been measured, and the underlying mechanics of tension based error detection and error correction remains unknown. In this study, we generated a gradient in tension over multiple isogenic budding yeast cell lines by genetically altering the magnitude of motor-based spindle forces. This allowed us, for the first time, to quantitatively elucidate the mechanics of tension based error detection pathway in mitosis. We found that a decreasing gradient in tension led to an increasing gradient in rates of kinetochore detachment and anaphase chromosome mis-segregration, with a corresponding gradient in metaphase times. Further, these tension-based cellular response gradients were abrogated in the absence of key error-correction pathway proteins. The underlying mechanism involves as increasing gradient in the degree of phosphorylation of proteins, comprising the load-bearing component of the kinetochore-microtubule interface, in response to a decreasing gradient in the magnitude of tension. We conclude that the cell is exquisitely tuned to the magnitude of tension as a signal to detect potential chromosome segregation errors during mitosis.

Table of Contents

List of Tables

List of Figures

Chapter One: Introduction

Mitosis in mammalian cells

Over the course of a complete cell cycle, a eukaryotic mother cell will duplicate its chromosomes, and distribute one copy of each chromosome to the two daughter cells that are formed when the mother cell divides. The act of distribution of chromosomes, termed as chromosome segregation, occurs during the M phase of cell division, more commonly known as mitosis. Mitosis proceeds in distinct stages (Fig 1A), starting with prophase, where chromatin starts condensing into recognizable chromosomes, comprised of two identical sister chromatids attached at to each at a region known as the centromere. Metaphase follows prophase, and is marked by the assembly of the mitotic spindle, formed from microtubules nucleated by the spindle poles (centrosomes in higher eukaryotes). At this stage, the duplicated chromosomes are aligned along the midzone of the mitotic spindle, in preparation for anaphase, the next stage of mitosis. At the onset of anaphase, the cohesion between sister chromatids breaks, and they are transported to the spindle poles in preparation for the final stages of mitosis (telophase) and subsequent splitting of the mother cell (cytokinesis). Failure to properly segregate results in aneuploidy, an improper chromosome number condition associated with certain cancers as well as birth defects (Kops et al., 2005)

This work focuses specifically on metaphase, in an effort to determine how the cell detects and corrects errors at this stage, in order to ensure proper segregation of chromosomes at latter stages of mitosis.

Structure of the mitotic spindle and the origin of forces

In budding yeast (*S.cerevisiae*), the primary model organism used in this study, the mitotic spindle is built from microtubules nucleated by the spindle pole bodies (Fig 1B). A class of microtubules, known as the kinetochore microtubules (kMts) make connection with the chromosomes at their centromeric region, through a proteinacious body called the kinetochore (Lampert and Westermann, 2011) that is built at the centromeres. A second class of microtubules, known as the inter-polar microtubules run along the length of the mitotic spindle but do not make contact with the chromosomes. The interpolar microtubules are organized into parallel bundles with opposite directionality (hence, anti-parallel bundles), by the action of passive and active bundling proteins. These regions of antiparallel bundling serve as localization points for a class of double headed, plus end directed motor proteins , known as the Kinesin-5 motors (Straight et al., 1998). The concerted action of these motors creates an outwardly directed force that tends to push the spindle poles away from each other, thus lengthening the spindle(Gatlin and Bloom, 2010). These forces are transmitted to the chromosomes via the kinetochore microtubules. Since the kinetochore microtubules make contact with the chromosomes at the centromeric region, these forces strongly affect the chromatin at the centromeric region, tending to stretch this region outwards (Wan and Cimini, 2012). Stretching of the centromeric chromatin resembles the stretching of a spring under an external force, and

like a spring, the chromatin exerts an inward force, known as tension, which tends to oppose the outward force (Chacon et al., 2014). Tension acts to stabilize the spindle against outwardly directed forces and prevents the spindle from growing too long and collapsing (Walczak and Heald, 2008).Tension may also be sensed by the cell to prevent errors in chromosome segregation (Pinsky and Biggins, 2005).This study focuses on the role of tension in preventing chromosomes mis-segregation.

Errors at metaphase and the role of tension.

A properly oriented chromosome has the two sister chromatids connected by microtubules to opposite spindle poles (Maresca and Salmon, 2010; Pinsky and Biggins, 2005)This ensures that when the cohesion between sister chromatids breaks at the onset of anaphase, the two chromatids are transported to opposite spindle poles, and are subsequently segregated to the two daughter cells.

Two types of error may occur during this process, both of which lead to chromosome mis-segregation if they are not corrected by the onset of anaphase (Elledge, 1996). One type of error is when a kinetochore is not attached to a microtubule. Such errors are detected by a kinetochore autonomous checkpoint, known as the Spindle Assembly Checkpoint, with the proteins Mad1 and Mad2 as key players (Vigneron et al., 2004). The checkpoint is on when Mad1 and Mad2 are enriched at kinetochores, and can work to catalytically activate soluble Mad2, which in turn sequesters a key activator of the metaphase to anaphase transition and delays the onset of anaphase (Han et al., 2013). This allows the cells time to correct the error

and establish an attachment with the proper kinetochore. The checkpoint is turned off when microtubules attach to the kinetochore, and dynein motors strip the Mad1-Mad2 complex away from the kinetochores by carrying them as cargo on the microtubules (Griffis et al., 2007; Varma et al., 2013). Thus, whether the checkpoint is turned on or off is intricately linked to the state of kinetochore-microtubule attachment, and the cell can read the state of attachment even though the operating principles are relatively simple.

The second type of kinetochore-microtubule attachment error is when a kinetochore is attached to a microtubule, but the attachment is improper. This type of error is the major focus of my thesis work. To ensure proper segregation at anaphase, a chromosome must have both kinetochores attached to microtubules emanating from opposite spindle poles. This mode of attachment is called amphitelic attachment, and a chromosome so attached is said to be "bi-oriented" (Shimogawa et al., 2010). However, a chromosome could be attached with both kinetochores attached to a single spindle (syntelic attachment), or, in organisms with multiple microtubules per kinetochore, with a single kinetochore attached to both spindle poles. Cells respond to these errors by destabilizing improper kinetochore-microtubules connections, thus leading to a detached kinetochore and allowing for a proper connections to subsequently form. (Hepperla et al., 2014; Khodjakov and Pines, 2010; Lew and Burke, 2003; Maresca and Salmon, 2010; Musacchio and Salmon, 2007; Pinsky and Biggins, 2005). However, the signal that the cell senses to detect these errors in orientation is not yet fully understood, and is the focus of this work.

We hypothesize that tension at centromeric chromatin may be sensed by the cell to read out the state of orientation. A properly oriented chromosome is expected to be acted upon by forces arising from opposite ends of the spindle, thus creating high tension in the centromeric

chromatin. On the other hand, because an improperly oriented chromosome is acted upon by forces primarily in one direction, the force acting to stretch the centromeric chromatin is expected to be much lower, and consequently tension at the centromeric chromatin is also expected to be commensurately lower (Fig.1C).

Sensing of tension could thus allow the cells to intricately link checkpoint signaling to the status of the error that a checkpoint is meant to sense.

Prior Research

The earliest reports of forces influencing the metaphase to anaphase transition used grasshopper spermatocytes in Meiosis I. In this work, the authors showed that the presence of a chromosome without a microtubule attachment (hence tensionless), could prevent a cell from entering anaphase. The authors were able to manipulate the chromosome using a calibrated micro needle and apply an external force in such a way that tension across the centromeric region increased. Cells with force applied to the chromosomes would rapidly enter anaphase (Li and Nicklas, 1997; Nicklas, 1997; Nicklas and Koch, 1969).

Similarly, it has been previously shown that the rate of metaphase to anaphase transition could be influenced by applying nano-Newton scale forces to the entire cell. In these experiments, mechanical clamps were used to apply a force to intact immobilized HeLa cells. Forces applied along the spindle axis, therefore acting against internal spindle forces and likely decreasing tension, led to delayed anaphase onset. Conversely, forces applied perpendicular to the spindle axis, thereby augmenting internal forces and likely increasing tension, could accelerate the cells into anaphase (Itabashi et al., 2012).

However, while these studies showed that the metaphase to anaphase transition could be affected by externally applied forces, they failed to elaborate the role of internal forces within the mitotic spindle.

Later work found that application of forces to praying mantid spermatocytes reduced the kinetochore staining of an epitope known as phoshpo 3F3/2 (Nicklas et al., 2001). Further work found that phospho 3F3/2 staining was increased when cells were treated with inhibitors of the kinsin5 motor Eg5, which is responsible for producing the outward forces in the mitotic spindles of higher eukaryotes. Inhibition of Eg5 in these studies led to mono-polar spindles, with the chromosomes expected to have near zero values of tension (Haase et al., 2017).

Together, these results suggested that cellular machinery reactive to external forces could also respond to changes in internal forces.

More recent work used tensionless chromosomes in budding yeast to evaluate the role of tension in mitotic error correction. Mutant yeast cells were allowed to enter metaphase with un-replicated chromosomes. With only one microtubule connection to one of the spindle poles, these chromosomes were effectively tensionless. These chromosomes triggered a mitotic checkpoint which delayed them in metaphase. Furthermore, a key effector of this checkpoint was demonstrated to be Aurora B, a protein known to play a role in the turn-over and correction of syntelic kinetochore-microtubule attachments (Biggins and Murray, 2001; Stern and Murray, 2001).

However, while the complete lack of tension can be sensed by the cell, it remains unclear whether a reduction in tension, as might be more physiologically relevant, can also be sensed by the cell to act as a readout of the correctness of chromosome orientation. Using the separation

of kinetochores as a proxy readout for tension , it has been demonstrated that reducing tension by treatment with the microtubule stabilizing drug Taxol triggers an Aurora B based mitotic checkpoint response. (Elowe et al., 2007; Waters et al., 1998). However, Taxol-mediated stabilization of microtubule dynamics may disrupt the error correction process, and the discovery that Taxol by itself may destabilize kinetochore-microtubule attachments, similar to an error correction response, complicates the interpretation of these studies (Rizk et al., 2009).

It was recently demonstrated that inhibition of Eg5 using a low doses of an inhibitory drug, STLC, led to decreased inter-kinetochore stretch, indicative of reduced, but not completely absent tension (Vallot et al., 2017) . These cells accumulated syntelic microtubule connections which required Aurora B activity to be resolved, suggesting that error correction was activated concurrently with low tension. However, the model system used was *Drosophila* oocytes in meiosis I, where the centromeric spring is made up of synaptonemal connections between two homologous chromosomes, rather than cohesion between sister chromatids of the same chromosome, as commonly observed in metaphase. Therefore tension is not built up between sister chromatids, as is the case at the mitotic metaphase. Thus while these results hint that low tension might be sensed at metaphase, the unreliability of inter-kinetochore spacings as a readout for tension, and meiosis specific differences in tension generation means that these results cannot be directly translated to mitosis.

Thus while there is evidence to suggest that cells may sense and respond to tension as a readout of chromosome orientation (Biggins and Murray, 2001; Stern and Murray, 2001), this issue remains controversial (Chmátal et al., 2015; Magidson et al., 2016; Ye et al., 2015).

Current Research Aims

While evidence suggests that the complete lack of tension can trigger a cellular response, there has been no conclusive evidence to demonstrate that changes in the magnitude of tension, such as might be physiologically relevant, can also bring about a cellular response.

Previous work has been severely hampered by the lack of a method to measure tension in live unperturbed cells. Most published research used inter-centromeric or inter-kinetohcore spacing as a proxy for tension (Jaqaman et al., 2010; Wargacki et al., 2010). However, as we have recently shown, spacings between centromeres/kinetochores does not necessarily correlate with tension (Chacon et al., 2014). Therefore, the aim of this work is to leverage direct measurements to quantitatively explore how cells sense changes in the magnitude of tension, and to provide a framework for how this can lead to downstream cellular responses that may be tuned to the severity of the tension defect.

In Chapter 2, I describe an assay to measure tension in live budding yeast cells. This optical assay allowed us to directly measure tension without using invasive means or causing large scale perturbations to the cells.

In Chapter 3, I describe methods to experimentally reduce tension in live yeast cells . These methods target outward forces against which tension is built up, and unlike previous work, does not alter microtubule dynamics, kinetochore structure, or require cell being studied to have un-replicated chromosomes. This allowed us to unambiguously explore the downstream effects of low tension.

In Chapter 4, I explore the initial response to low tension, that is the creation of detached kinetochores. This assay is based on the principle that erroneous attachments have been

demonstrated to lead to detached kinetochores as they are turned over in favor of properly oriented ones (Nezi and Musacchio, 2009)and if our hypothesis holds true, we would expect a similar response in low tension cells. In Chapter 4, I also explore the mechanistic aspects of the tension response by identifying the key kinase that mediates the cellular low tension response. Finally, I test whether this response scales with tension in a dose dependent manner.

In Chapter 5, I test the consequences of detachments. We show that these detachments delay the progression from metaphase to anaphase in a Spindle Assembly Checkpoint dependent manner. This delay likely allows the cell time to re-attach its kinetochores, which leads to high rates of chromosome mis-segregation in the absence of a delay response. As in the previous section, I show that this response also varies with tension in a dose dependent manner.

In Chapter 6, I use simulations to ask what mechanism can best explain the dose dependency of the above cellular responses to decreasing tension. Our simulation rules, based on previously published reports, used only two simple assumptions. 1)phosphorylation of outer kinetochores proteins increases with decreasing tension, and 2)the probability of detachment increases with increasing phosphorylation of these proteins. I found that introducing only these two simple rules into the simulation allowed me to recapitulate my experimental data to a high degree of accuracy.

Lastly, in chapter 7, I use proteomics approaches to directly demonstrate, for the first time, that the level of phosphorylation of a key protein, Dam1, increases with decreasing tension. This was a result predicted by my simulation and provided my with strong experimental support for our simulation methods.

Taken together, our results form a complete and quantitative picture of tension sensing in the cell, and open up exciting possibilities for future work.

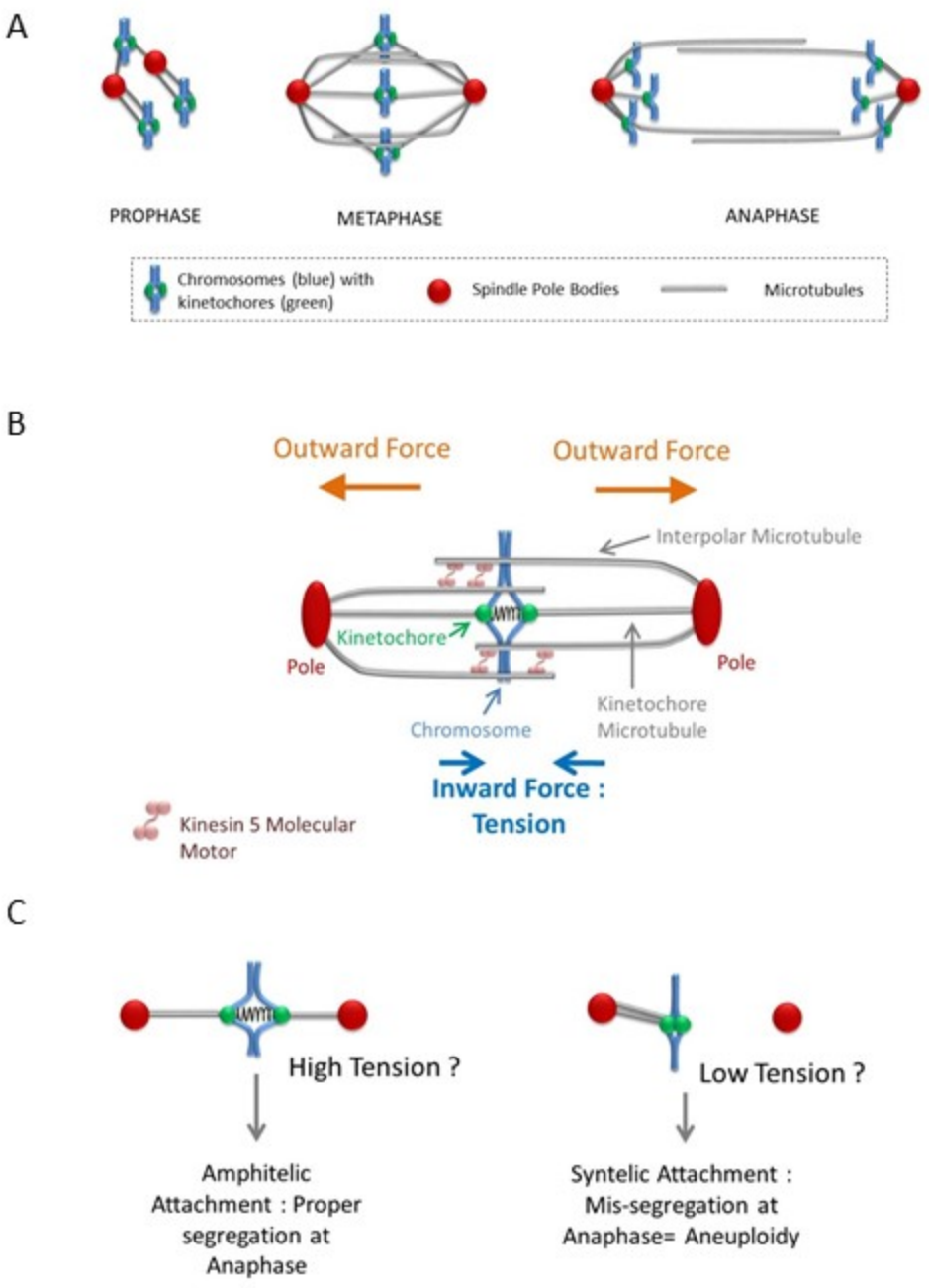

Figure 1 : Cells may sense the magnitude of tension at metaphase to prevent chromosome mis-segregation

Figure 1 : Cells may sense the magnitude of tension at metaphase to prevent chromosome mis-segregation. A) Cartoon showing stages of mitotic progression from prophase through anaphase in budding yeast cells. B) Cartoon of a budding yeast mitotic spindle showing the directionality of motor derived forces, and chromatin derived tension. C) Schematic showing proper and improper state of attachment, and how tension may be low when attachment is improper.

Chapter Two: Measurement of tension in live budding yeast cells.

Introduction

To test the idea that the magnitude of tension at metaphase is sensed by the cell as a readout of the state of orientation of the chromosomes, we devised an optical, non-invasive assay to directly measure tension in live budding yeast cells. Previous attempts to measure tension have employed means such as physical manipulation of the chromosomes with micro needles, or have used the spacing between centromeric or kinetochore labels as an approximate readout for tension. Micro-needle manipulations are difficult to perform in the lab, requiring specialized setups or techniques, and are invasive and disruptive to the cell. The use of inter-kinetochore or inter-centromeric spacings is complicated by the fact that these spacings do not directly correlate with tension under all circumstances, as we previously reported (Chacon et al., 2014).

To accurately and non-invasively measure tension in live budding yeast cells, we took advantage of an assay devised in the lab which relies on high resolution, fast time scale imaging. This assay takes advantage of the fact peri-centromeric chromatin, or the chromatin the spans the region between the kinetochores of the two sister chromatids, behaves like a spring (Stephens et al., 2011)(Fig 2A). As previously discussed, this inter-kinetochore spring region stretches under the influence of applied forces, and relaxes to its original length when force is absent (Chacon et al., 2014; Wan and Cimini, 2012). This stretching and relaxation can be observed in strains which had 33 lacO repeats inserted proximally to the centromeres on chromosome 3. A lacI-GFP fusion was expressed in these cells, which localized to the lacO repeats, thus forming two distinct puncta in each cell, which can be visualized under the microscope. These puncta mark the two centromeres, and consequently, the two ends of the spring formed by the centromeric chromatin. These two dots will be referred to as LacO spots from now on. Most of our experimental cells also have SPC110, a component of the spindle pole bodies tagged with the red fluorescent protein, mCherry, representative image is shown in (Fig 2C).

Physical basis of the assay and results

Tension is built up in the stretched chromatin spring against the forces acting on it (Pearson et al., 2001). It has been previously reported that this spring behaves as a linear Hookean spring over the spatial range of expansion relevant to this study (Chacon et al., 2014).

Thus, tension ($F_{tension}$) was estimated via the equation for Hooke's law, as follows (Fig 2B):

$$F_{tension} = \kappa(\Delta x - \Delta x_{rest}) \qquad \text{(Eqn 1)}$$

Here, κ is the stiffness of the inter-kinetochore spring, and κ was estimated using the methods summarized below. Δx_{rest} is the rest length of the inter-kinetochore spring, i.e., the distance between the sister centromere lacO-lacI-GFP spots when no forces are pulling them apart. For Δx_{rest} we used previously published values that were estimated as described in (Chacon et al., 2014) using cells treated with Nocodazole to depolymerize microtubules, thus eliminating all forces on the chromosomes. For spindles treated with Nocodazole, the separated sister centromere lacO-lacI-GFP spots collapse to a single diffraction-limited spot, and so the rest length was estimated as the theoretical microscope resolution, based on the numerical aperature of the microscope lens (Chacon et al., 2014). Δx is the average metaphase stretch distance of the inter-kinetochore spring, as represented by the average distance between lacO-lacI-GFP spots with properly bioriented kinetochores at metaphase (Fig 2C). The stretch distance was measured by collecting many still images of metaphase spindles, and then by evaluating the center-to-center distance between the two lacO-lacI-GFP spots on pairs of sister chromatids of the same chromosomes (Chr 3 in our studies).

Estimation of spring stiffness

The final measured parameter that was required in order to estimate tension was the stiffness of the inter-kinetochore spring (κ) (Fig 2D). The inter-kinetochore spring stiffness is a measure of its resistance to force-induced stretching, and is expressed in unites of its spring constant (k). Here, a stiffer spring i.e that is more resistant to force induced stretching will have a higher spring constant than a spring that is less resistant to force induced stretching i.e is less stiff. The general principle involved in the measurement of spring stiffness is that the spring constant (κ)

is reflected in the range motion of the lacO-lacI spots with respect to each other under the influence of the thermal energy that is available to move them at a given temperature.
The range of motion is quantified as the variance ($<\sigma^2>$) in the relative spacings of the lacO spots over increasing amounts of time, and the spring constant(κ) is related to the variance ($<\sigma^2>$) according to the relationship given by Eqn.2.

$$\kappa = \frac{k_B T}{<\sigma^2>} \qquad \text{(Eqn 2)}$$

k_BT is the amount of energy that is available to move the lacO-lacI-GFP spots on the centromeric spring, which is the Boltzmann constant (k_B) multiplied by the temperature (T).

Thus, in order to use this relationship, the measured variance in motion of the lacO-lacI-GFP spots should reflect thermal forces, and not active, directed forces by microtubules and motors. In our previous work, we reasoned that thermal forces occur on a fast time scale relative to active forces, and so we collected rapid time-lapse movies (33 frames/s) of the LacI-GFP tags to visualize the rapid fluctuations of the tags with respect to each other over small time scales of ~2 seconds (Fig 2E). We also verified this approach using drugs to halt active forces, and demonstrating that the measurements yielded identical results. (Chacon et al., 2014). After movie collection, the center of each LacO-LacI GFP spot for every time frame was accurately localized using 2D Gaussian fitting, thus limiting measurement noise to ~20 nm, and the distance between pairs of lacI-GFP tags on sister chromatids (Δx_i was measured for each time point (Fig 2F).

To quantify the variability in distance between pairs of sister lacO-lacI-GFP tags over time, the distance measurements were converted to Mean Squared Displacement (MSD) values for increasing intervals of time (Δt), as follows:

$$MSD = \frac{1}{n}\sum_{j=1}^{n}\left[\sum_{i=j}^{j+\left(\frac{\Delta t}{t_{step}}\right)-1}\Delta x_i\right]^2 \qquad \text{(Eqn 3)}$$

Here, t_{step} is the time between image frames in the movies (30 ms under our imaging conditions), and *n* is the number of displacements within the time interval (eg, $n=\Delta t/t_{step}$).
At very short time steps (Δt <0.5 s), the MSD vs ∆t plots shows a linear increase (Fig 2G, left). This reflects free diffusion of the LacO-LacI-GFP spots, relative to each other, driven by thermal forces. However, because the LacO-LacI-GFP spots are linked to each other via the centromere spring, the tags will not diffuse away from each other indefinitely. Rather, their diffusive, thermally driven motion will be constrained by the stiffness of the centromere spring connecting them. This results in the MSD vs ∆t plot to plateau at time intervals where Δt>0.5 s. This characteristic plateau is represented in simulated data (Fig 2G left), and in a representative MSD vs Δt plot of data collected from experimental yeast strains (Fig 2G. right). The height of this plateau ($<\sigma^2>$) is proportional to the relative stiffness of the centromere spring. A softer spring allows for greater movement of the LacO-LacI-GFP tags relative to each other (larger $<\sigma^2>$), while a stiffer spring allows less relative movement (smaller $<\sigma^2>$). At time steps significantly larger than 2-3 sec, the MSD vs Δt plot would show a quadratic increase in MSD value. This behavior arises under the influence of active, directed forces resulting from kinetochore microtubule dynamics (Fig 2G, left, yellow shaded area of curve). However, largely because of high frame rates employed, and low duration of imaging, our measurements do not extend into

this regime for individual cells, and motion we capture is thermal in origin. For further justification of this method, see Materials and Methods, and references cited. (Chacon et al., 2014)

The MSD values were then plotted for increasing time intervals (up to ~2 sec maximum) and the plots were used to find the plateau value of MSD, ($\langle\sigma^2\rangle$), where $\langle\sigma^2\rangle = MSD_{plateau} - MSD(\Delta t_1)$. A representative plot of MSD vs Δt shows a plateau characteristic of constrained diffusion (Fig 2G, right). Here, the height of this plateau above the Y intercept represents ($\langle\sigma^2\rangle$). To calculate the stiffness of the inter-kinetochore spring (κ), the value for $\langle\sigma^2\rangle$ was then substituted into Eqn. 2.

The average centromeric spring constant in 15 pN/μm in unperturbed budding yeast cells, and the average stretch distance is 0.5 μm. This indicates that the average tension built in each chromosome is 5pN (Fig 2H), as calculated by substituting values into Eqn. 1. Importantly, tension is substantial, well above the minimum thermal noise threshold, and so is large enough to potentially provide a tension-based mechanical signal to ensure the fidelity of chromosome segregation during mitosis in budding yeast. However, whether the magnitude of tension is read out by the cell, and transduced into an important chemical signal during mitosis remains an open question.

Discussion

Here, we present a method for measuring tension in live budding yeast cells using an assay that is exclusively optical in nature. This assay avoids invasive physical manipulation of the cell, and provides the first direct measurement of tension in unperturbed cells. While previous attempts

at measuring tension largely relied on inter-kinetochore spacings as a readout for tension (Jaqaman et al., 2010; Wargacki et al., 2010) , these methods can be inaccurate if the specific experimental conditions alter the physical properties, and hence the spring constant of the centromeric chromatin (Chacon et al., 2014). We did not make any assumptions regarding the state of the chromatin spring in all our experimental strains, and measured tension in all of them. We note that our measurements yield both stiffness and tension values that are in the same order of magnitude as previously published measurements , and match the best estimates for these parameters in budding yeast cells (Salmon and Bloom, 2017). This method, combined with multiple isogenic tension mutants (discussed below), allowed us, for the first time, to quantitatively demonstrate how cells sense tension, and how they react to changes in the magnitude of tension.

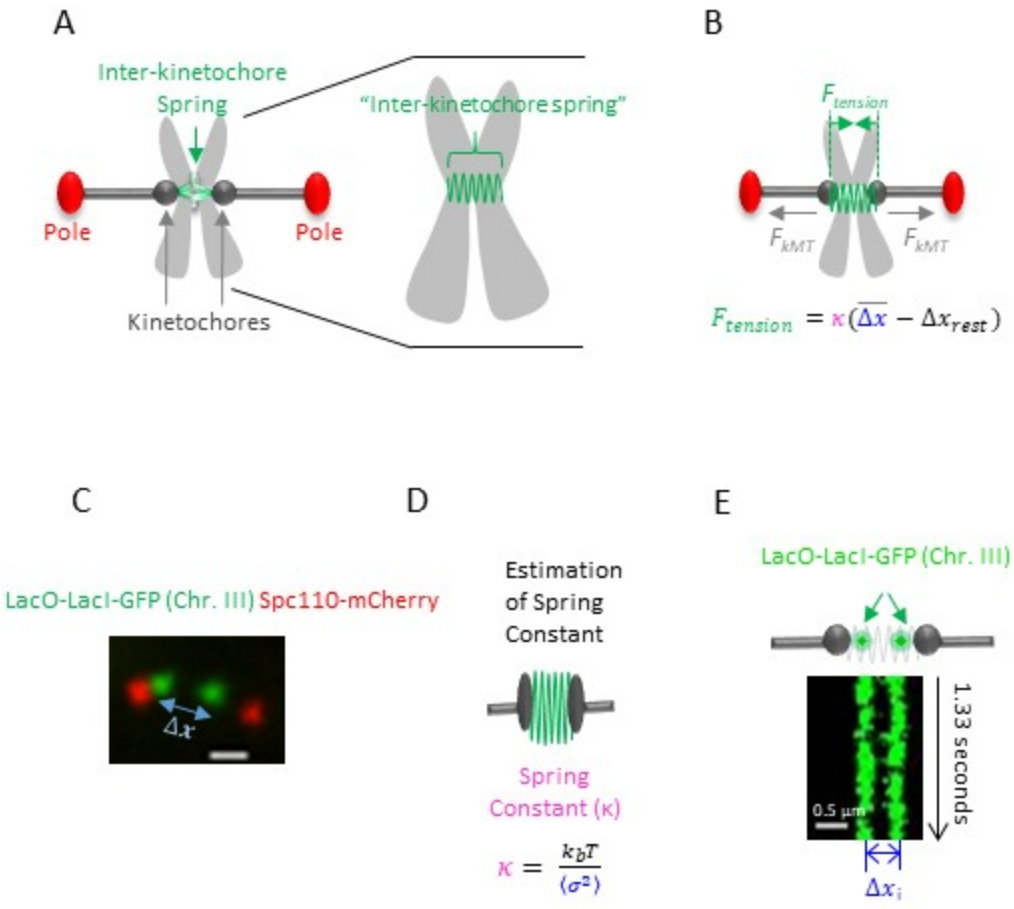

Figure 2 : Measurement of Tension

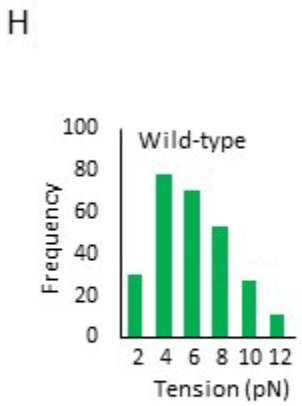

Figure 2 (Contd.) : Measurement of Tension

Figure 2: Measurement of tension (A) Left: Cartoon of a budding yeast metaphase spindle. Right : Blow-up cartoon of duplicated sister chromosomes, including the inter-kinetochore spring that connects the two sister kinetochores. (B) $F_{tension}$ (green) represents tension that is generated in the inter-kinetochore spring as a result of molecular motors that push apart the spindle poles (red). (C) Representative micro-graph of an experimental strain showing tagged centromeres and spindle. Inter centromere spacing (Δx) is labeled. (D) Cartoon of centromeric spring with equation relating motion of the spring to the stiffness (E) Representative kymograph showing how lacO-lacI-GFP sister spot spacings change over time using fast time-lapse imaging. Kymograph shows 40 frames imaged at 30 fps. (F) Representation of fluorescence intensity of the lacO-lacI-GFP centromeric labels along the spindle axis as a histogram (green bars), and subsequent Gaussian fitting to accurately determine the center of each spot (red line)). To estimate spring constant, the distance between the two spots is determined, and designated as Δx_i. This is repeated for all time points of a movie. (G) Mean squared displacement (MSD) vs time step size curve for wild type *S. cerevisiae* cells (blue arrow shows calculated $\langle\sigma^2\rangle$ value . (H)Distribution of tension magnitudes as measured in wild-type cells (see materials and methods and (Chacon et al., 2014)).

Chapter Three: Genetic means of reducing tension in budding yeast cells.

Introduction

Tension in the centromeric chromatin is built up against the outwardly directed forces acting on the chromosomes. These forces are derived both from the action of plus directed kinesin 5 motors(Gatlin and Bloom, 2010) and from microtubule dynamics (Grishchuk et al., 2005). While it is possible to make completely abrogate tension by allowing unreplicated chromosomes to enter anaphase (Biggins and Murray, 2001; Pinsky et al., 2006), reducing tension by small, physiologically relevant amounts has proven to be a technical challenge. Previous attempts have focused on altering microtubule dynamics in an attempt to reduce tension. Since tension is partly built up against pulling forces exerted by de-polymerizing microtubules (Grishchuk et al., 2005), the microtubule stabilizing drugs, most notably Taxol, have been used to treat cells in order to reduce tension(Joglekar, 2016) . While Taxol treated cells have been shown to have reduced inter-kinetochore spacings (Magidson et al., 2015), and to accumulate the 3F3/2 phospho-epitope associated with low tension, these experiments have been plagued with several factors that make the interpretation of the results difficult. Significantly, taxol treated cells have been shown to retain Mad2 at kinetochores, implying that taxol leads to detached or low occupancy kinetochores (Waters et al., 1998). This is in contrast to cases with un-replicated (hence tensionless) chromosomes, where kinetochore-microtubule connections are eventually

stabilized and Mad2 is absent from the kinetochores before anaphase onset.(O'Connell et al., 2008) Contradictory data suggests that kinetochore microtubule connections are hyper-stabilized when cells are treated with higher concentrations of taxol. Therefore erroneous kinetochore –microtubule connections cannot be turned over and corrected. (Yang et al., 2009). These data taken together demonstrates that while taxol may reduce tension, the cellular processes that occur downstream of low tension to correct potential errors are significantly altered, and hence cannot be effectively studied. The fact that taxol treatment also brings about large scale changes in kinetochore structure further complicates the interpretation of these studies (Wan et al., 2009).

We chose to target the kinesin 5 molecular motors which exert outward forces against which tension is built up (Straight et al., 1998). These outward forces are an integral part of the spindle, as evidenced by the fact that inhibition of the single kinesin 5 molecular motor in higher eukaryotes, Eg5, leads to spindle collapse (Kapoor et al., 2000). Cells lacking Eg5 function are not viable. Budding yeast however, have two different kinesin 5 molecular motors stemming from a genome duplication event, Kip1 and Cin8 (Hildebrandt and Hoyt, 2000). These motors perform similar roles at metaphase, and yeast cells with any one motor knocked out are viable. We targeted these motors in an attempt to reduce tension (Fig. 3A, left). This method does not target microtubule dynamics, chromosome structure or replication, or kinetochore structure, and we reasoned that this could provide a powerful tool for quantitatively evaluating the sensitivity of the cell to tension as a mechanical signal at metaphase.

Kinesin 5 molecular motors localize to stretches of anti-parallel microtubule overlap. These regions of overlap are created by bundling proteins, both passive and active, acting to remodel

the spatial geometry of microtubules (Hepperla et al., 2014). We targeted a passive bundling protein, Ase1 (Janson et al., 2007; Schuyler et al., 2003), in a further attempt to reduce tension. The absence of Ase1 leads to increased spacing between spindle microtubules (Gardner et al., 2008), facilitating a reduction in the dynamic crosslinking of Cin8 and Kip1 between antiparallel microtubules. We predicted that reduced Kinesin-5 crosslinking would lower the Kinesin-5 mediated outward force generation in the metaphase spindle without any change in the overall expression levels of the Kinesin-5 motors.(Fig 3A, right) (Hepperla et al., 2014).

Results

To test whether the mutants as described above would lead to reduced metaphase tension, we first verified our previous results by measuring average metaphase tension in the wild-type budding yeast cells ($F_{tension}$= 4.9 pN) (Chacon et al., 2014), and then used our published protocol to measure metaphase centromere tension for each of the mutants (Fig. 3B, bottom)
We found that each of the mutants had a unique tension magnitude in metaphase, such that *cin8Δ* cells had the lowest average tension (Fig. 3B, bottom, 2.8 pN), while *ase1Δ* and *kip1Δ* cells had average tension magnitudes that were between the wild-type and *cin8Δ* values (Fig. 3B, bottom, *ase1Δ* = 3.3 pN; *kip1Δ* = 4.0 pN). Tension varied significantly across all the strains ($F_{3,1069}$ = 70.31, p<0.0001), and, importantly, the average tension magnitudes trended downward across the motor mutants (p < 0.0001 wild-type vs *kip1Δ*, p < 0.0001 *kip1Δ* vs *ase1Δ*, and p = 0.003 *ase1Δ* vs *cin8Δ*) . This tension gradient thus provided a tool for exploring the response of the cell to moderate, step-wise decreases in the average metaphase tension magnitude.

For the *kip1*Δ and *ase1*Δ strains the low tension was reflected solely in the decreased lacO spacings. (Fig 3B, top). The MSD vs Δt plots (Fig 3C), and consequently the spring constant (Fig 3D) remained constant in all of these mutants. Interestingly, we observed that the *cin8*Δ cells had a reduced spring constant as compared to the wild type (Fig 3F), as well as the other mutant cells, with the MSD vs t plots for *cin8*Δ cells exhibiting a higher plateau (Fig 3E). We verified that the reduction in stiffness was also observed in Δ*cin8* cells in the 15D strain background, as well as the W303 strain background, which we used for all of our studies.(Fig 3G).

We also characterized two conditional mutants of Δ*cin8*. The pgal-cin8 strain had the *cin8* gene expressed under the galactose promoter, and gene expression was repressed when the cells were shifted to media containing glucose. The degron-cin8 strain had the cin8 gene tagged with an N-terminal degron, and had the E3 ubiquitin ligase UBR1 expressed under the gal promoter (Kotwaliwale et al., 2007). These cells rapidly degrade cin8 when shifted to media containing galactose. Both conditional mutants, when shifted to conditions that either repressed or degraded *cin8,* exhibited spring constants (Fig 2H), and average tension values (Fig 2I) which were identical to *cin8*Δ cells.

Discussion

Reducing tension by small, physiologically relevant amounts in live cells has been technically challenging. We targeted kinesin 5 motors to reduce outward forces against which tension is built up. We also targeted a bundling protein that helps recruit these motors to the mitotic spindle. Each mutant had reduced tension as compared to wild type. More importantly each

mutant had different values of average tension, such that tension decreased in a graded manner across the full range of isogenic mutants. This gave us a means to test quantitatively if the cellular response to tension was graded in nature, i.e whether the magnitude of the downstream cellular response corresponds to the value of tension in a dose dependent manner. We note that the decreasing values of tension across our motor mutants were correlated with decreased average spacings between lacO-lacI-GFP spots in these strains (Fig 3B, top), consistent with the idea that centromere tension is proportional to inter-kinetochore spring stretch distance. However, this relationship does not hold true for all cases, and the low stiffness in the *cin8*Δ and conditional mutant strains of cin8 contributes significantly to the low value of tension observed in these strains. This underlines the importance of measuring tension in cells using our method, and shows that solely relying on inter-kinetochore/centromere distances as a readout for tension can be un-reliable.

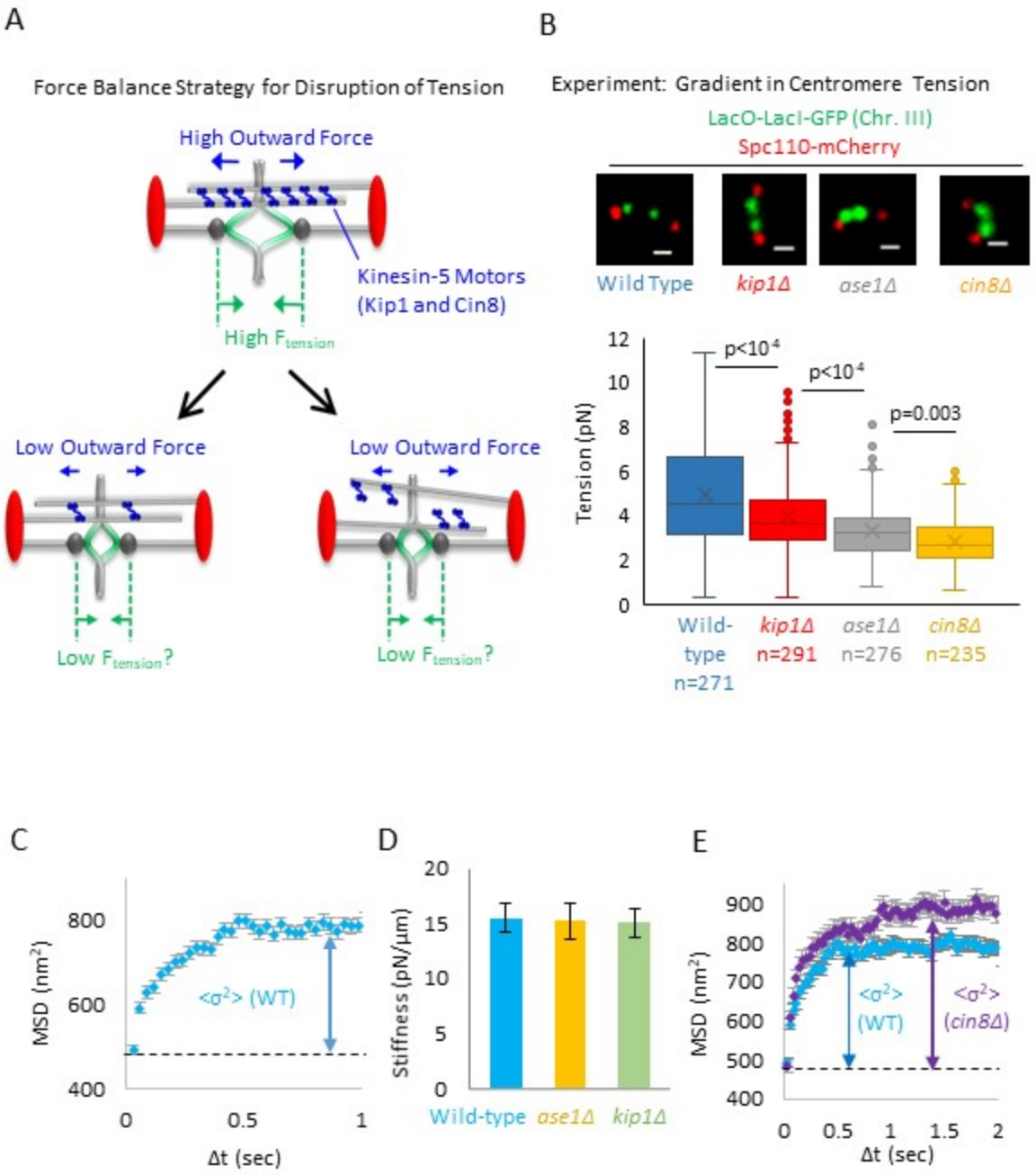

Figure 3 : Generation of a gradient in tension and characterization of conditional tension mutants.

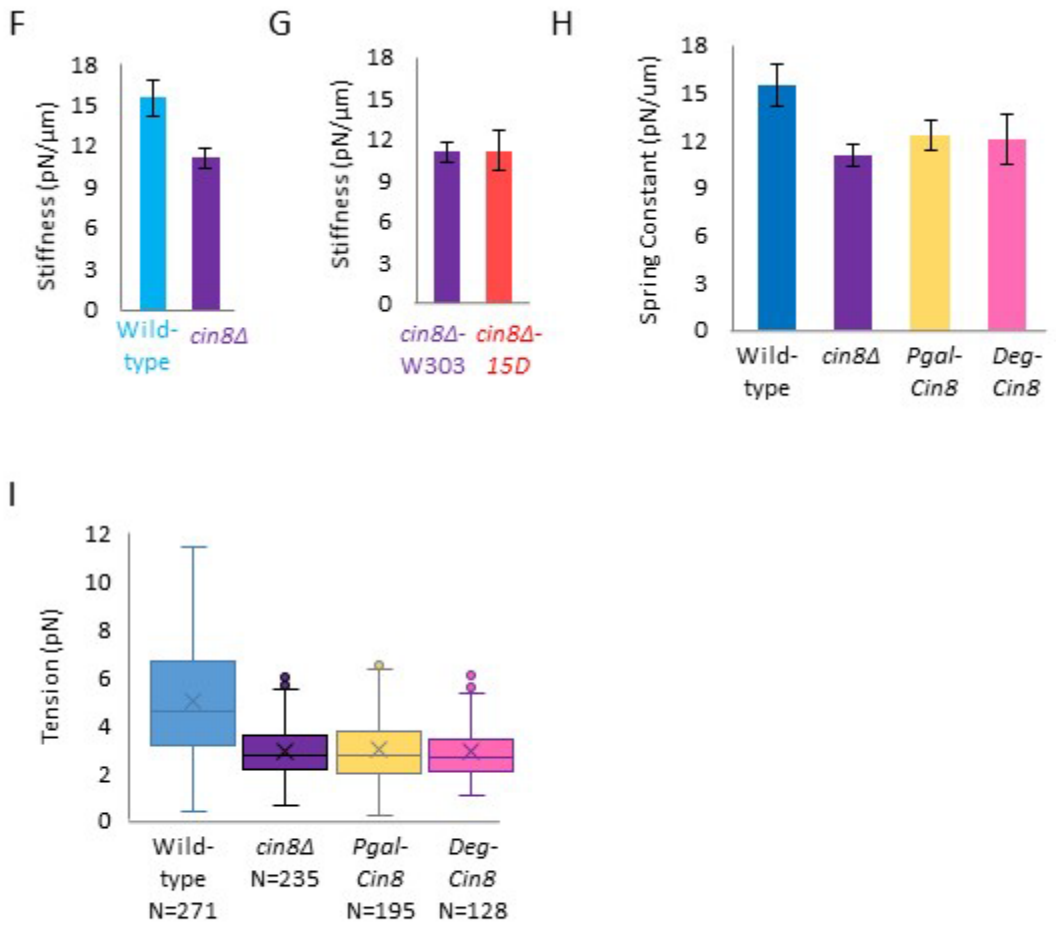

Figure 3 (contd.) : Generation of a gradient in tension and characterization of conditional tension mutants.

Figure 3 : Generation of a gradient in tension and characterization of conditional tension mutants. (A) Cartoon highlighting a strategy for suppressing tension by experimentally reducing outward forces. Top: Generation of outwardly directed spindle forces by Kinesin-5 motors (blue) that crosslink antiparallel spindle microtubules (grey) leads to tension (green). Bottom-left: One strategy for reducing outward motor-based forces was to selectively delete Kinesin-5 motor protein genes. Bottom-right: A second strategy involved disrupting microtubule bundling (Fig. S1A), therefore reducing the force-producing crosslinking of Kinesin-5 motors. (B) Top:

Representative images of lacO spot spacings in wild type and mutant budding metaphase spindles (scale bar, 500 nm). Bottom: Measured tension in these strains reveals a decreasing gradient in average metaphase tension (p-values calculated from a least squares means multiple comparison procedure using a Bonferonni correction; bars: quartiles, marker: average, box: 1st quartile, line in center of box: median). (C)) Mean squared displacement (MSD) vs time step size curve for wild type *S. cerevisiae* cells (blue arrow shows calculated $<\sigma^2>$ value. (D) Comparison of spring constants for wild-type, *kip1Δ*, *ase1Δ* cells. (E) MSD vs time-step size curves comparing wild type (blue) with the *cin8Δ* mutant (purple). (blue and purple arrows show calculated $<\sigma^2>$ values. (F) Quantification of the spring constant in *cin8Δ* mutant as compared to wild-type cells. (G) Comparison of spring constants in *cin8Δ* mutants from two different strain backgrounds. All panels: error bars=SEM. (H) Comparison of spring constants in Cin8 conditional mutants as compared to wild-type and *cin8Δ* cells. Pgal-cin8 cells were grown and imaged in glucose to repress Cin8 expression for comparison to Deg-Cin8. Deg-Cin8 cells were imaged with induction of Cin8 degradation. (I) Comparison of average tension magnitudes in wild-type, *cin8Δ* and Cin8 conditional knockout cells ($F_{2,554} = 0.25$, $p = 0.77$, *cin8Δ vs* Pgal-Cin8 *vs* deg-Cin8).

Chapter Four: Low Tension leads to detachments in a dose dependent manner

Introduction

The cellular response to erroneous kinetochore-microtubule connections is well documented. The initial response to such errors leads to destabilization of incorrect kinetochore microtubule

connections(Lampson et al., 2004; Pinsky et al., 2006; Sarangapani et al., 2013; Tanaka et al., 2002). This allows for the microtubules to detach from the kinetochores, and a proper attachment to be made in its place. This is a stochastic process, and may take multiple rounds of re-attachment and detachment before a proper connection is made (Cimini et al., 2006). Once a proper connection is made, it is selectively stabilized and the cell is allowed to enter anaphase(Akiyoshi et al., 2010; King and Nicklas, 2000) .

This process is exemplified at the beginning of mitosis. In budding yeast cells especially, nearly all chromosomes make erroneous connections at the earliest stages of metaphase, when the two spindle pole bodies have just been formed through a duplication event, and the mitotic spindle is being assembled. At this stage multiple rounds of de-stabilization has been observed prior to all chromosomes being properly oriented at metaphase (Jin et al., 2012; Marco et al., 2013; Tanaka et al., 2002). This effect can also be observed in cells derived from higher organisms, including mammalian and human cells, recovering from kinesin 5 inhibition (Straight et al., 1998). When treated with drugs that inhibit the activity of kinesin 5 motors, the spindle collapses into a monopole. In the absence of a complete spindle, the chromosomes are nearly tensionless, and accumulate errors in orientation. When the drug is washed out and the spindles allowed to re-form, orientation errors are corrected via de-stabilization of erroneous connections followed by establishment and stabilization of proper connections.

This process has also been observed to play a crucial role in the correction of erroneous connections in mid to late metaphase (Cimini et al., 2006). Since the creation of detachments are an integral part of error correction at metaphase, and we hypothesize the signal that the cell senses to initiate error correction is low tension, we reasoned that our low tension motor and motor recruitment mutants may also have detached chromosomes. We asked whether the

incidence of these detached chromosomes scales with tension in a dose dependent manner. (Fig 4A)

We took advantage of the relative simplicity of our model system to devise an optical assay to score for detachments. In higher eukaryotes, the presence of multiple microtubules per kinetochore makes it experimentally challenging to score single detachment events. In *S.cerevisiae* however, the single microtubule connection per kinetochore (O'Toole et al., 1999)makes scoring for detachments relatively straightforward.

In cells with labeled centromeres (lacO spots) and pole markers, attached chromosomes are under tension and the spindle displays two distinct lacO spots. Detachment of the single microtubule connection leads to an instant release of tension, analogous to treatment with the microtubule destabilizing drug Nocodazole (Chacon et al., 2014). The two lacO spots collapse to a single, diffraction limited spot, usually located towards one end of the spindle. (Figure 4B) The relative incidence of these detachment events across our tension mutants can be easily scored. These detached spots were not included in our tension analysis.

Results

Incidence of detachment increases with decreasing tension in a dose dependent manner.

To determine the relative rates of kinetochore detachment in our wild-type and tension mutant cells, we collected images of individual metaphase spindles for each strain (n > 500 images for each strain), and then counted the number of metaphase spindles with two separated lacO spots (e.g., attached kinetochores), and the number of spindles with a single, off-axis lacO spot

near to one pole (e.g., at least one kinetochore detached) (Fig. 4B). We found that the ratio of detachments varied significantly across strains ($X^2 = 248.13$, $p < 0.0001$), and was higher in all of the motor mutant strains as compared to wild type cells (Fig. 4C; $p \leq 0.0006$ all comparisons). There was a statistically significant increase in detachments even when average tension was decreased by as little as 0.9 pN ($X^2 = 11.91$, $p = 0.006$, wild type to *kip1Δ*). Strikingly, the detachment rate scaled with tension in a dose dependent manner: the mutants with lower average tension magnitudes had a higher detachment rate, and those with higher tension had a reduced detachment rate (Fig 4C; $z = -15.49$, $p < 0.0001$, Cochran-Armitage trend test). These results suggest that metaphase cells are exquisitely sensitive to tension, leading to a population-wide, dose-dependent kinetochore detachment response that directly scales with the magnitude of average tension. We validated our detachment assay by comparing the relative intensity of the single diffraction limited lacO spots with the separated lacO spots. The diffraction limited, detached lacO spots had an average intensity approximate twice that of separated lacO spots (Fig 4D), as might be expected given that the single spots derive from two, overlapping lacO spots.

Tension-dependent detachment gradient depends on Aurora B activity

We then asked whether our observed tension-dependent detachment phenotype could be a specific consequence of the cell activating its error correction machinery in response to low tension. We focused on Aurora B, a serine-threonine kinase which has been shown to play a key role in the error correction process.(Lampson and Cheeseman, 2011) Aurora B has been shown to de-stabilize erroneous kinetochore-microtubule connections, and hence plays a key role in

creating detached kinetochores which are an important intermediate in the error correction process(Pinsky and Biggins, 2005). Absence of Aurora B leads to large scale chromosome mis-segregation (Biggins et al., 1999), and Aurora B may be activated at metaphase in response to low tension (Biggins and Murray, 2001; Liu et al., 2009).

The budding yeast homolog of Aurora B is *ipl1*. This protein is essential and cannot be knocked out (Keating et al., 2009; Muñoz-Barrera and Monje-Casas, 2014; Pinsky et al., 2006). To test the role of *Ipl1* in mediating the observed tension-dependent detachment gradient, we used a well-characterized temperature sensitive allele, *ipl1*-321, which leads to inactivation of *Ipl1* when cells are shifted to the restrictive temperature of 37 ^{o}C (Biggins et al., 1999; Keating et al., 2009).

However, *ipl1* performs multiple roles during multiple stages of mitosis. One of its key roles is the turnover of syntelic attachments formed during the earliest stages of metaphase, before the mitotic spindle has fully formed. De-activation of *ipl1* in an asynchronous culture leads to the accumulation of syntely into late stages of metaphase (Marco et al., 2013). Since syntely and detachment cannot be distinguished effectively using our optical assay (Liu et al., 2008), we needed to devise a way to minimize syntely at metaphase in order to unambiguously study the role of *ipl1* in tension sensing. To prevent these defects from complicating our analysis, we depleted *Cdc20*, a protein essential for the metaphase to anaphase transition (Chao et al., 2012), in order to arrest our cells in metaphase before shifting temperatures to 37 °C to deactivate *Ipl1* . This allows time for early mitotic syntely to be resolved before *ipl1* is de-activated. *Cdc20* depletion was accomplished by shifting yeast cells expressing *Cdc20* under the control of the Met promoter into media containing high concentrations of methionine and cysteine, thus repressing *Cdc20* expression, as previously described. (Keating et al., 2009).

Using this protocol, we first evaluated both metaphase detachment and tension in cells that were arrested in metaphase via Cdc20 depletion and then shifted to 37 °C (Fig. 4F (circles, detachment rates); Fig 4E (tension)). Differences in mean tension remained statistically significant within the Cdc20 arrested strains ($F_{3,665}$ = 124.05, p<.0001, Fig. 4E), and, similar to our previous observations (Fig. 4C), we observed a trend of increasing metaphase detachment rates with decreasing average tension for the control Cdc20 metaphase-arrested cells (Fig. 4F, circles; z = -12.79, p < 0.0001, Cochran-Armitage trend test). These results were also similar to cells that had the *ipl1*-321 allele, but were measured at the 26 °C permissive temperature, allowing Ipl1 to remain active (Fig 4H, z = -8.14, p < 0.0001, Cochran-Armitage trend test). Importantly, we then measured tension and detachment rates for *Cdc20* metaphase-arrested cells that harbored the *ipl1*-321 allele, and that were shifted to 37 °C, thus inactivating *Ipl1* (Fig. 2F (crosses, detachment rates); 4G (tension)). We found that although tension differences remained statistically significant across the *ipl1* restrictive tension mutant strains (Fig 4G, $F_{3,1151}$ = 139.43, p<.0001), the dose-dependent relationship between detachment and tension was lost when ipl1 was deactivated (X^2 = 0.27, p = 0.966) (Fig. 2F, crosses). Here, the cells with inactivated Ipl1 had a characteristic basal detachment rate that remained constant regardless of tension magnitude (Fig 4F, crosses). For these experiments we used the cin8-degron strain, as *cin8*Δ *ipl1-321* double mutant cells exhibit synthetic lethality.

Discussion

Our metaphase kinetochore detachment data provide the first direct evidence that small reductions in tension activate the cellular error correction machinery in a dose dependent manner.

The advantages of using multiple mutants with different values of tension is clear, without multiple strains with differing values of mean tension, the dose dependent nature of the cellular response low tension response could not be detected.

Ipl1 has been previously implicated in tension-dependent error correction (Biggins and Murray, 2001; Cimini et al., 2006; Hauf et al., 2003; Kallio et al., 2002; Lampson and Cheeseman, 2011; Lampson et al., 2004). Inactivation of *ipl1* in all of our tension mutants returns the detachment frequency to a similar basal level, regardless of the value of tension, or the specific tension mutant used. These results demonstrate that the tension dependent detachment we observe is a specific consequence of the error detection machinery being activated in response to decreasing tension.

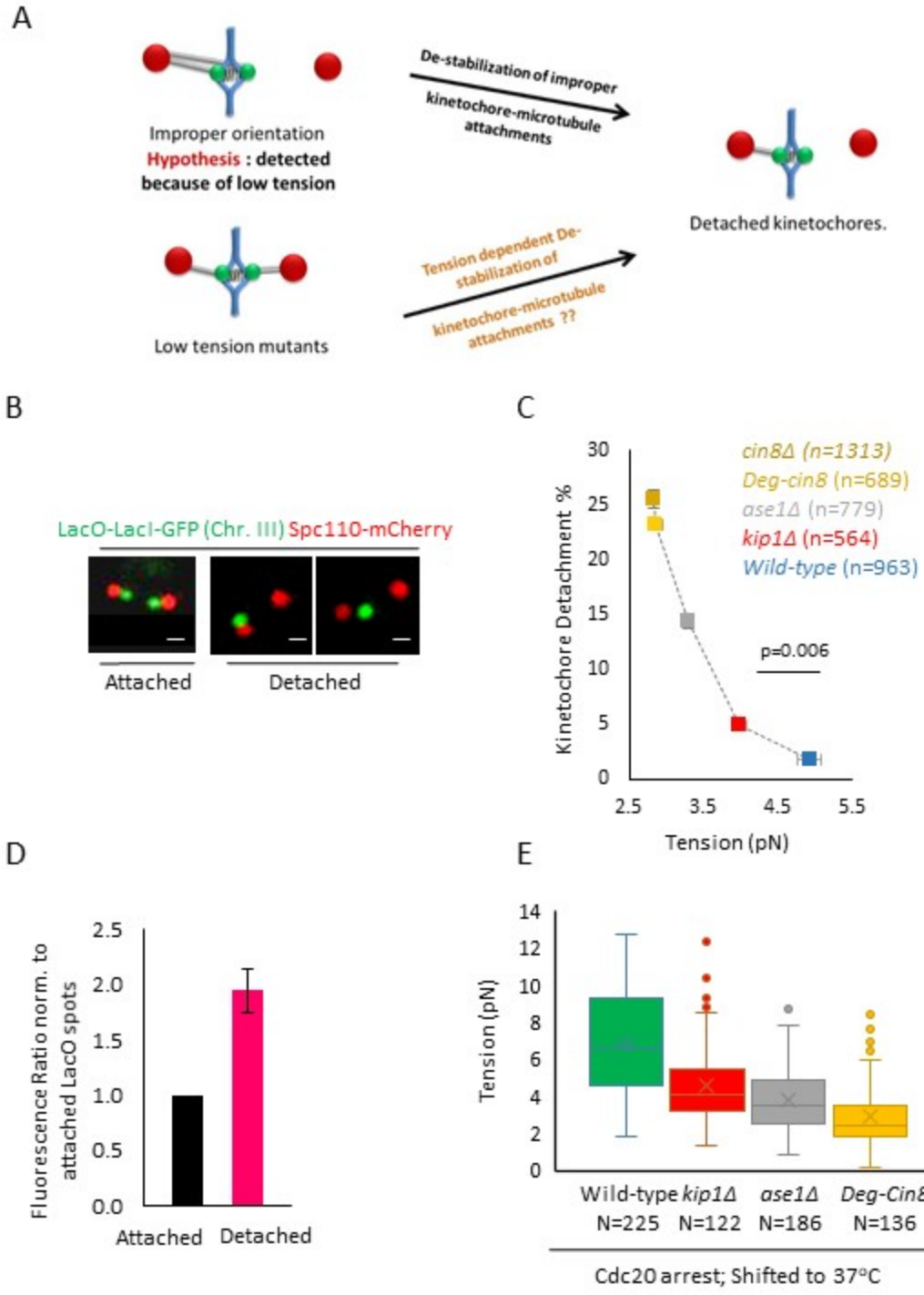

Figure 4 : Estimation of Detachment rates in low tension mutants, and identification of the kinase responsible for detachments

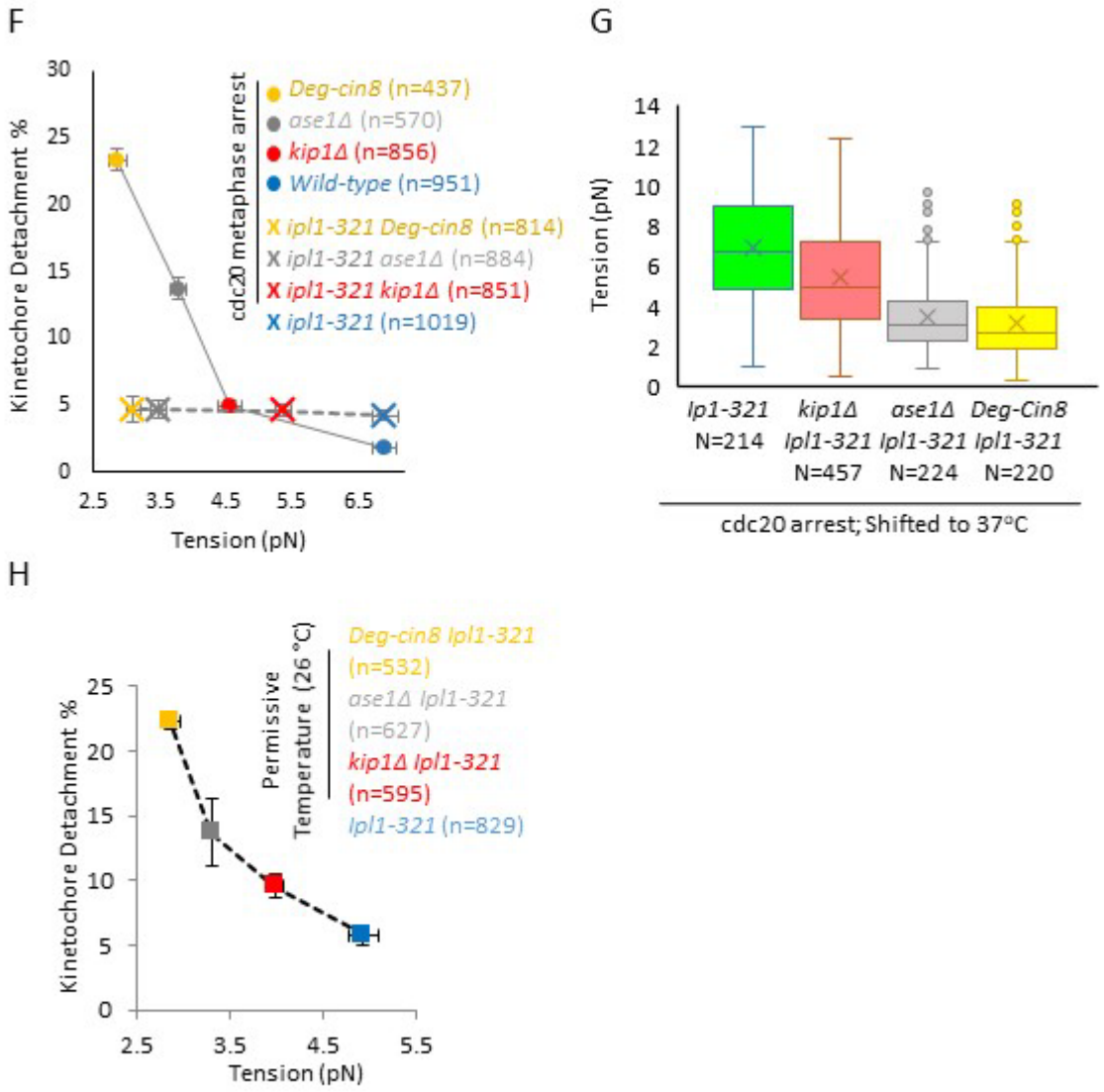

Figure 4 (contd.) : Estimation of Detachment rates in low tension mutants, and identification of the kinase responsible for detachments

Figure 4 : Estimation of Detachment rates in low tension mutants, and identification of kinase responsible for detachments. (A)Cartoon demonstrating a potential cellular response to low tension: a low metaphase tension (left) could lead to an increase in detached kinetochores (right). (B) Top: Representative images of lacO-lacI-GFP spots in cells with properly attached kinetochores (left), and detached kinetochores (right) in budding yeast (scale bars, 500 nm). (C)

Detachment rate vs tension in wild type and mutant strains. The tension and detachment rate in the Degron-Cin8 cells (dark yellow) was similar to that in *cin8Δ* cells (light yellow). The detachment rate increased substantially with decreasing tension ($z = -15.49$, $p < 0.0001$, Cochran-Armitage trend test), and the detachment rate was significantly increased even when average tension was decreased by as little as 0.9 pN ($X^2 = 11.91$, $p = 0.006$). (D) Measurement of lacO-lacI-GFP intensity in cells with separated lacO-lacI-GFP spots (attached), and cells with a single diffraction-limited spots (detached) (scale bars 500 nm). (E) Quantification of tension in cells that were arrested with Cdc20 depletion and shifted to 37 °C ($F_{3,665} = 124.05$, $p<.0001$). (F)Detachment rate vs tension in wild type and tension mutant strains in Cdc20 arrested cells at 37 ^{o}C (circles; tension measurements in Fig. S2D-E), and detachment rate vs tension in wild type and tension mutant strains in cells that harbored the *ipl1-321* allele, and that were Cdc20 arrested at 37^{o}C (crosses; tension measurements in Fig. 4G). The detachment rate increased substantially with decreasing tension for the Cdc20 arrested cells ($X^2 = 169.70$, $p < 0.0001$), but the inactivation of Ipl1 abrogated this dependence ($X^2 = 0.27$, $p = 0.966$). All panels: error bars=SEM. (G) Quantification of tension in cells harboring the *ipl-321* allele, arrested with Cdc20 depletion and shifted to 37 °C ($F_{3,1151} = 139.43$, $p<.0001$). (H) Dependence of detachments on magnitude of tension in cells harboring the ipl-321 allele, at permissive temperature (26 °C) ($z = -8.14$, $p<0.0001$, Cochran-Armitage trend test).

Chapter Five: Detachments lead to metaphase delay and chromosome mis-segregation.

Introduction

In eukaryotic cells, a chromosome with a detached kinetochore will likely be mis-segregated at anaphase. To prevent this, detached kinetochores trigger the Spindle Assembly Checkpoint (Lew and Burke, 2003; Musacchio and Salmon, 2007). As previously discussed, this checkpoint is based on the key players, Mad1 and Mad2. Mad1 is a kinetochore localized protein and forms a complex with Mad2 at unattached kinetochores (Moyle et al., 2014; Waters et al., 1998). The Mad1-Mad2 complex at the kinetochore catalytically converts soluble, inactive Mad2 to soluble, active Mad2. Active Mad2, along with Bub1 and BubR1(Mad3) forms a multi-protein complex known as the Mitotic Checkpoint Complex (MCC)(Chao et al., 2012) . The Mitotic Checkpoint complex sequesters Cdc20, and prevents it from forming a complex with the APC/C. APC/C is an E3 ubiquitin ligase, and when activated upon forming a complex with Cdc20, rapidly ubiquitinates Cyclin B and Securin, leading to their degradation(Collin et al., 2013; Juang et al., 1997; Lu et al., 2014). Degradation of cyclin B de-activates the metaphase specific cyclin dependent kinase, and degradation of securing allows a protein known as separase to degrade a subunit of cohesion, thereby releasing the connection between two sister chromatids (Hirano, 2006). Degradation of Cyclin B and Securin rapidly and irreversibly brings about anaphase onset(Cohen-Fix and Koshland, 1997). Conversely, in the presence of unattached kinetochores, the sequestration of cdc20 delays the onset of anaphase. This allows the cell time to re-attach these kinetochores, and prevent mis-segregation of chromosomes at anaphase(Dick and Gerlich, 2013).

Given that we observed increased rates of detachment in our tension mutants, we went on to ask the following questions. Firstly, do tension mutants spend more time in metaphase, and does the time spent in metaphase correspond to the magnitude of tension? Secondly, is there more chromosome mis-segregation observed in the tension mutants, and does the incidence of mis-segregation scale with tension in a dose dependent manner ?

Results

Tension mutants spend more time in metaphase than wild type cells.

To test whether there was a metaphase delay in our tension mutants, we measured metaphase time by performing time-lapse imaging in yeast cells in which we followed the spindles poles of yeast cells from pole duplication to anaphase (Fig 5A, top), and then plotted spindle length vs time for each of our cells (Fig 5A, bottom). These plots were then used to measure the time spent in metaphase (Fig 5A, bottom, metaphase time marked in gray).

To verify that cells with metaphase-like spindle lengths were indeed in metaphase, we quantified the average nuclear Pds1 intensity as a marker for mitotic progression (Lu et al., 2014), using cells with representative spindle lengths for the wild-type strain and each of the mutants. While we could readily detect a sharp drop-off in Pds1 intensity in anaphase cells, as has been previously reported (Lu et al., 2014), our mutant cells with metaphase-like spindle lengths did not show reduced Pds1 intensity (Fig 5B). We therefore confirmed that cells with metaphase-like spindle lengths were indeed in metaphase, and so we then measured metaphase time for the wild-type and mutant cells.

We found that our low tension mutants spent more time in metaphase than wild type cells (Fig 5C, circles; $F_{4,187} = 7.77$, $p<0.0001$), and, consistent with our metaphase detachment results, the average metaphase time also scaled with tension in a dose-dependent manner (Fig 5C, circles; $p<0.0001$, linear trend). To test whether the observed metaphase delays were a specific consequence of Spindle Assembly Checkpoint activation, we evaluated metaphase times in the *mad2Δ* background cell lines, which did not have a functional Spindle Assembly Checkpoint. Since the *cin8Δ-mad2Δ* cells were not viable, so we used the previously described Cin8-degron mutant for these experiments (Kotwaliwale et al., 2007). Consistent with the idea that the observed metaphase delays were mediated by Mad2, the gradient in average metaphase times was no longer observed in the tension mutants when Mad2 was absent (Fig 5C, crosses; $F_{3,126} = 0.45$, $p=0.72$), even though a gradient in kinetochore detachment rates was still observed (Fig. 5D). These results suggest that the primary response of the cell to low tension is the creation of detachments, and that the Spindle Assembly Checkpoint performs a protective function downstream of this primary response by delaying cells in metaphase. Furthermore, Spindle Assembly Checkpoint function is not needed to create detachments in response to low tension.

Tension mutants exhibit increased chromosome mis-segregation, which is exacerbated in the absence of Mad2.

To detect mis-segregated chromosomes during anaphase in synchronized *mad2Δ* cells, we adapted a previously described assay (Miller et al., 2016) in which we released mutant and wild type cells from an alpha factor arrest, and once the population had entered anaphase, we fixed

the cells, stained with DAPI. We then scored cells for unequal distribution of green Chr. III lacO spots into the nuclei of each daughter cell (Fig 5E, yellow boxes). We found that in the *mad2Δ* strain background there was a dose-dependent increase in anaphase mis-segregation rates with decreasing tension (Fig. 5F, triangles; $z=-6.16$, $p<0.0001$, Cochran-Armitage trend test). Of note, our observed anaphase chromosome mis-segregation rates in *mad2Δ* cells (Fig. 5F, triangles) were similar to our metaphase kinetochore detachment rates as described above (Fig. 4C). Persistent low tension in our tension mutants therefore led to large-scale mis-segregation of chromosomes in the *mad2Δ* background cell lines, due to increased rates of metaphase kinetochore detachment. As would be expected, the overall magnitude of anaphase chromosome mis-segregation was lower with Mad2 present as compared to our *mad2Δ* cells (Fig 5F, circles ; $X^2 = 36.61$, $p < 0.0001$, Mad2 background main effect). However, as noted above, the metaphase kinetochore detachment rate was unaffected by the presence or absence of Mad2 (Fig 5D; $X^2 = 0.09$, $p = 0.76$, Mad2 background main effect).

Because *cin8Δ-mad2Δ* cells were not viable, we used the previously described Cin8-degron mutant (Kotwaliwale et al., 2007) for these experiments as well.

Discussion

Our tension mutants spent more time in metaphase than wild type cells, with time spent in metaphase increasing with decreasing tension in a dose dependent manner. The tension dependent metaphase delay is no longer observed when Mad2 is additionally knocked out, showing that detached kinetochores created in response to low tension are detected by the Spindle Assembly Checkpoint.

This delay likely allows the cell time to remake kinetochore-microtubule connections prior to anaphase onset. This is supported by the fact that while the rate of chromosome mis-segregation increases in a dose dependent manner with decreasing tension, the overall rates of mis-segregation across all tension mutants is dramatically increased when Mad2 is absent. Interestingly, the dose dependent relationship between tension and mis-segregation is still observed when Mad2 is absent, but occurs at a greater level. Strikingly, the rates of chromosome mis-segregation in a *mad2*Δ background closely matches the rates of detachment observed in the tension mutants.

These results allow us to come up with a mechanistic view of tension sensing, where low tension triggers the creation of detachments as the first response. The Spindle Assembly Checkpoint detects these detachments, and delays cells at metaphase to prevent these detached chromosomes from being mis-segregated. This system is not perfect, and a low number of chromosomes escape surveillance and are mis-segregated. However, when the Spindle Assembly Checkpoint is inactivated, cells go through metaphase regardless of the detachment status of their chromosomes, and thus almost every chromosome which is detached at metaphase, is mi-segregated at anaphase.

So far, our data taken together shows that low tension leads to a multi-step process of detachment, metaphase delay and re-attachment with occasional chromosome mis-segregation, and that the magnitude of all these processes scale with tension in a dose dependent manner.

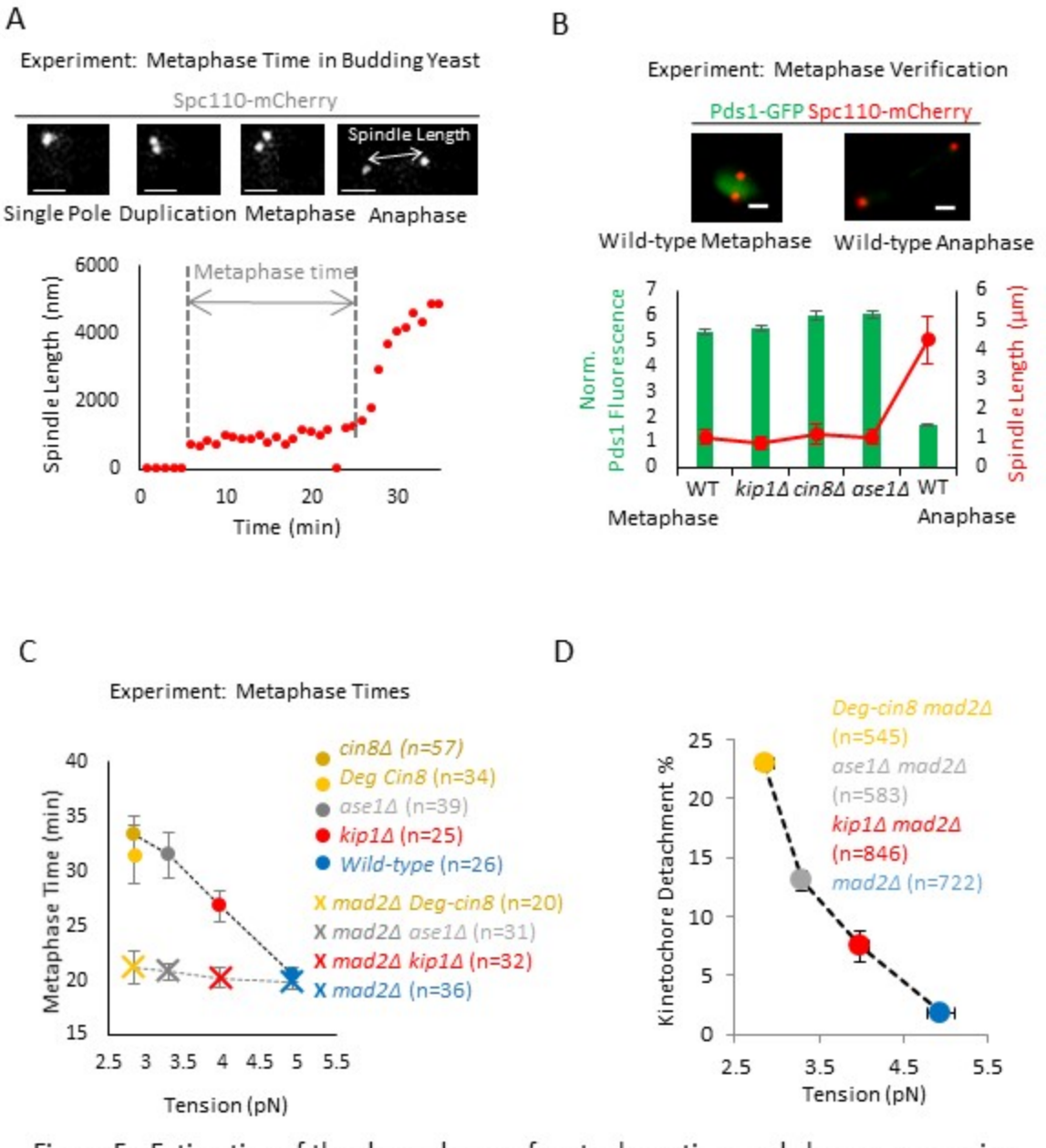

Figure 5 : Estimation of the dependence of metaphase time and chromosome mis-segregation on tension

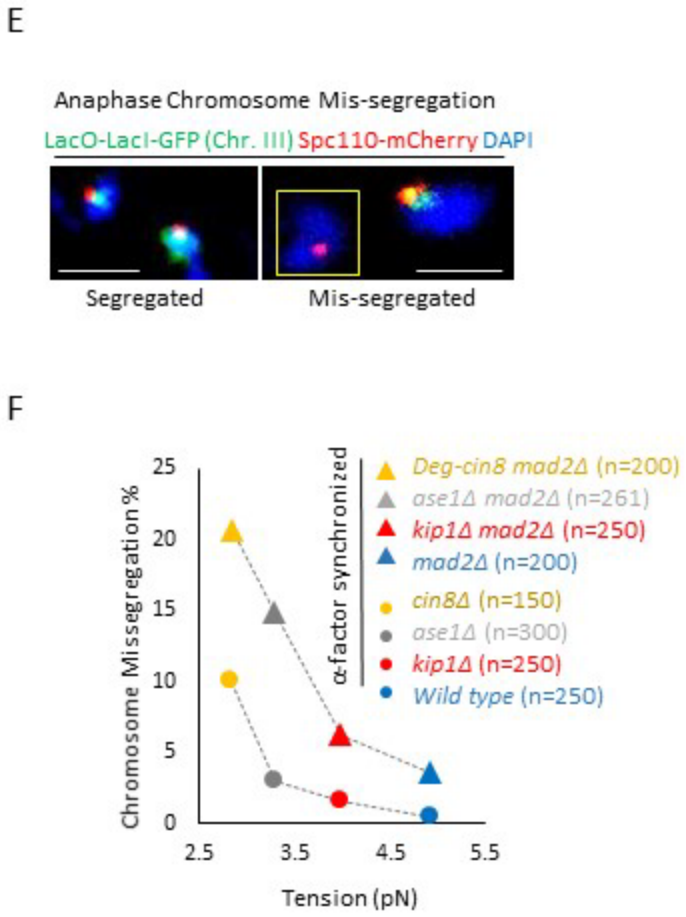

Figure 5 (contd.) : Estimation of the dependence of metaphase time and chromosome mis-segregation on tension

Figure 5 : Estimation of the dependence of metaphase time and chromosome mis-segregation on tension (A) Top: Representative images of budding yeast Spc110-mCherry spindle pole markers taken from a time lapse series of a cell going through mitosis (scale bars, 1500 nm). Bottom: Plot of spindle length vs time. Recorded metaphase time shown in grey. (B) Top: Representative images of Pds1-GFP fluorescence in budding yeast cells at metaphase (left) and anaphase (right) (scale bars, 1500 nm). Bottom: Quantification of Pds1-GFP intensity at metaphase-like spindle lengths in wild type and mutant cells. This plot suggests that the spindle

lengths designated as metaphase in the spindle length vs time experiments were indeed in metaphase, since Pds1-GFP fluorescence was still present in high levels. (C) Average metaphase time vs tension for the wild-type and tension mutant cells (circles; $F_{4,187} = 7.77$, $p<0.0001$, linear trend $p <0.0001$), and metaphase time for the wild-type and tension mutant cells when Mad2 was additionally knocked out (crosses, corresponds to the detachment data in figure 4C). Metaphase times remain near wild-type levels for all mutants in the absence of Mad2 ($F_{3,126} = 0.45$, $p=0.72$), despite reduced tension and increased incidence of detachments (Fig. 4D). (D) Dependence of detachments on magnitude of tension in the *mad2Δ* mutant background ($z = -11.29$, $p<0.0001$, Cochran-Armitage trend test). All panels: error bars=SEM. (E)Representative images of lacO-lacI-GFP spots (green) and chromosomes (blue, DAPI) in anaphase cells with proper chromosome segregation (left), and representative images of lacO-lacI-GFP spots (green) and chromosomes (blue, DAPI) in anaphase cells with improper, missegregated chromosomes (right) (pole with missing lacO-lacI-GFP spots shown in yellow boxes) (scale bars, 2500 nm). (F) Anaphase chromosome missegregation rate vs tension in a *mad2Δ* strain background (triangles; $z=-6.16$, $p<0.0001$, Cochran-Armitage trend test). Note that detachment rates were similar regardless of the presence or absence of Mad2 (Fig. S2H). The anaphase missegregation rate was reduced in cells with normal Mad2 expression (circles; $X^2 = 36.61$, $p < 0.0001$).

Chapter Six: Simulations with tension-dependent kinetochore phosphorylation rate constant can explain detachment gradient

Introduction

To investigate a mechanism for how the kinetochore detachment rate could gradually increase in response to decreasing magnitudes of tension, we used a simulation-based approach. The rules for the simulation are based on the most widely accepted model for how error correction may be dependent on tension sensing.

Error correction and tension sensing are both thought to occur at the level of individual kinetochores. (Fig 6A). The key process is the phosphorylation of NDC80 and Dam1 proteins by the Aurora B kinase. NDC80 and Dam1 are the main proteins responsible for connecting the kinetochore to the microtubule, and hence are the load bearing members of the kinetochore-microtubule interface (Joglekar et al., 2010; Powers et al., 2009). Both NDC80 and Dam1 are targets of Aurora B (Akiyoshi et al., 2009a; Gestaut et al., 2008), and the affinity of NDC80 and Dam1 for microtubules is greatly reduced when they are phosphorylated(Tien et al., 2010; Zaytsev et al., 2015). This causes detachments to occur with greater probability and allows for efficient error correction(Sarangapani et al., 2013). It has been shown that Aurora B dependent phosphorylation of NDC80 and Dam1 is increased in cases of an orientation error, which is likely to be a low tension condition(Keating et al., 2009; Welburn et al., 2010). Based on these lines of evidence, we introduced two rules into our simulation : 1) decreasing tension would lead to an

increased substrate phosphorylation rate constant ; 2) Increased phosphorylation levels of NDC80 and Dam1 increases the probability of detachment. We then tested if these two simple rules could recapitulate the dose dependency of detachments on tension that was experimentally observed.

We note that the exact manner by which low tension leads to increased phosphorylation of Aurora B substrates is still under debate. The consensus in the field holds that under high tension, the kinetochore stretches, mediated by a hinge domain in the long arm of NDC80, and this physically pulls Aurora B substrates away from the kinase which is localized to the inner centromere . (Fig 6A, left) This allows protein phosphatases such as Glc7 (PP1) to de-phosphorylate NDC80 and Dam1, and hence stabilize the kinetochore-microtubule connection. Conversely, under low tension, the kinetochore is thought to contract (Fig 6A, right), thus allowing Aurora B access to its substrates and increasing their phosphorylation level (Lesage et al., 2011; Sarangapani et al., 2013; Tien et al., 2010; Welburn et al., 2010; Westermann et al., 2007; Yamagishi et al., 2014). While this model is supported by some lines of evidence , most notably the fact that artificially tethering Aurora B to outer kinetochore, thereby mimicking conditions of low kinetochore stretch, can activate error correction regardless of tension (Liu et al., 2009). However, the exact relationship between kinetochore stretch and tension remains a subject of debate, and efforts to relate kinetochore stretch with low tension have led to results which vary depending on the methods used to reduce tension, or to measure intra-kinetochore stretch (Liu et al., 2012; Magidson et al., 2016; Maresca and Salmon, 2009; Suzuki et al., 2011, 2014). Given the controversy surrounding the mechanism of tension sensing, our model makes

no assumptions about the exact mechanism by which decreasing tension leads to an increased substrate phosphorylation rate.

Results

Our simulations were centered around an individual kinetochore-microtubule attachment structure with N_{sites}= 50 phosphorylation sites (results are similar for N_{sites} = 2-150) (Cheeseman et al., 2001, 2002, 2006; Joglekar et al., 2006). Each site could be phosphorylated (Fig. 6B, left, red), or dephosphorylated (Fig. 6B, left, green). In the simulation, the rate of switching between phosphorylation states at each site was regulated by rate constants, in which k_{phos} was the phosphorylation rate constant per site (s^{-1}), and k_{dephos} was the dephosphorylation rate per site (s^{-1}). Importantly, the phosphorylation rate constant decreased exponentially with increasing tension, according to:

$$k_{phos} = k_{phos,0} e^{-\lambda F_{tension}} \qquad \text{(Eqn. 4)}$$

Where $k_{phos,0}$ was the basal phosphorylation rate constant in the absence of tension, $F_{tension}$ was the tension (pN), and λ was the scaling factor that determined the influence of tension on the phosphorylation rate constant (pN^{-1}), such that for λ=0, there was no influence of tension on the phosphorylation rate constant, and for λ>0, increased tension would act to exponentially decrease the phosphorylation rate constant (Fig. 6B, right, λ=1 pN^{-1}).

Thus, for each separate simulation, a different tension was imposed on the kinetochore-microtubule attachment structure. At each time point (Δt_{step}=0.01 s), the individual phosphorylation sites stochastically switched between a phosphorylated or dephosphorylated state, according to the rate constants as described above. Thus, with increasing tension, a smaller number of sites tended to be phosphorylated (Fig 6C, top-right).

To directly compare our simulation results to experiments, we then allowed detachment events to occur, where the probability of a kinetochore detachment event (pr_{det}) depended upon the fraction of phosphorylated sites (Tien et al., 2010; Zaytsev et al., 2015):

$$pr_{\det} = \beta\left(\frac{N_{phos}}{N_{sites}}\right) \qquad \text{(Eqn. 5)}$$

Here, N_{phos} represented the number of phosphorylated sites, and β was a sensitivity factor that linearly scaled the fraction of phosphorylated sites with the probability of detachment. In order to allow the simulation to achieve a steady-state level of detachments for each given tension value, any detached kinetochore was automatically reattached at a similar tension magnitude after an elapsed time that was consistent with published observations (Kalinina et al., 2013) (see Appendix B : Simulation Methods for details)

Using the rules and the parameter values as described above, the simulation recapitulated the experimentally observed relationship between detachment and tension (Fig 6C, bottom). This result was most sensitive to the parameter value for λ, which relates the sensitivity of k_{phos} to

tension (Fig. 6D, Eqn. 4). For example, when $\lambda=0$, k_{phos} was insensitive to tension (Fig. 6D, left, red), and a gradient in detachment rate with tension was not observed (Fig. 6D, right, red). The best fit between experiment and simulation was for $\lambda=1\ pN^{-1}$ (Fig. 6D, left, cyan), which led to a clear gradient in detachment rate vs tension that was similar to experimental results (Fig. 6D, right, dotted grey line is experimental data; parameter sensitivity analysis for other simulation parameters in Appendix B : Simulation Methods). Thus, we conclude from our simulations that a tension-dependent kinetochore phosphorylation rate constant could explain our experimentally observed gradient in detachment rates with tension.

Discussion

We used computational modeling to further investigate a potential mechanism for our experimentally observed dose-dependent response to low tension, which also provides a pathway for future explorations. We found that our probabilistic model could faithfully recapitulate our experimental observations of a dose-dependent detachment response to decreasing average tension magnitudes if (1) the kinetochore phosphorylation rate was tension dependent, and (2) the strength of the kinetochore-microtubule binding interface was directly reduced by an increasing fraction of phosphorylated sites. Our model thus establishes a quantitative framework with clear assumptions to explain our experimentally observed dose-dependent cellular response to changes in metaphase tension. Interesting future work will involve testing these assumptions, for example, by predicting and experimentally evaluating changes to the tension-dependent detachment rate gradient in mutants with altered numbers of active kinetochore phosphorylation sites(Akiyoshi et al., 2009b; Sarangapani et al., 2013; Tien

et al., 2010). As previously mentioned, the underlying physical mechanism of a tension-dependent kinetochore phosphorylation rate may involve the kinetochore itself stretching under high tension (Maresca and Salmon, 2010), and limiting the accessibility of Aurora B to its substrates (Fig 6A) (Liu et al., 2009; Maresca and Salmon, 2009), but this particular mechanism remains controversial (Dumont et al., 2012; Magidson et al., 2016). Thus, interesting future work could also center on the origin of a tension-dependent phosphorylation rate constant, since we predict that alterations in component(s) that mediate a tension-dependent kinetochore phosphorylation rate would directly alter our experimentally observed gradient in detachment rate as a function of tension.

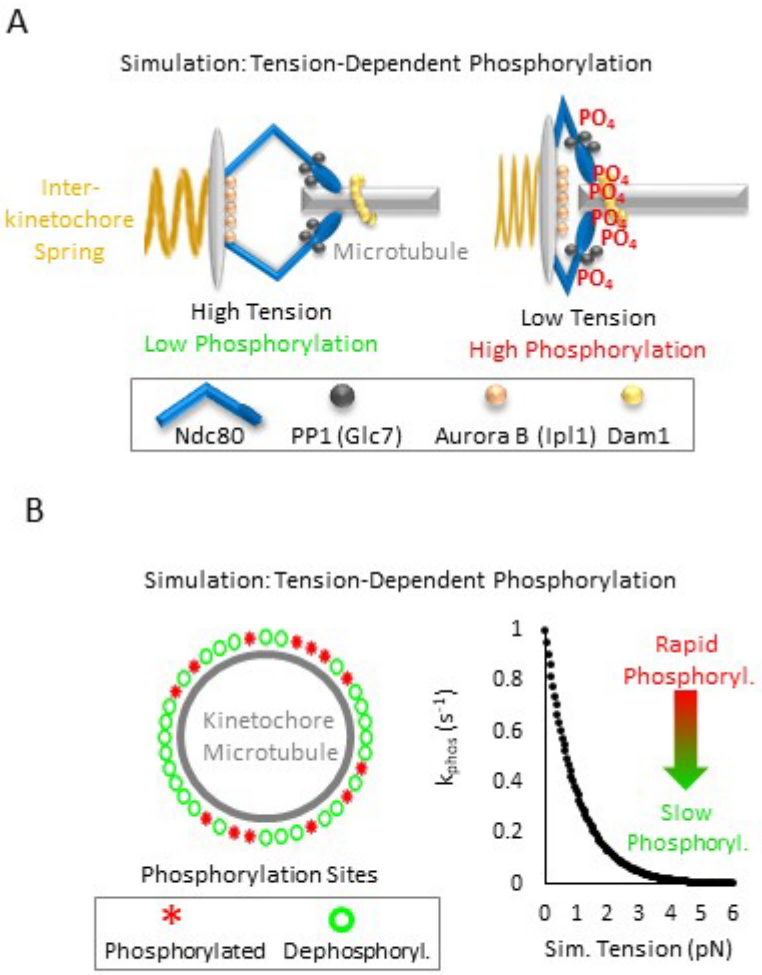

Figure 6 (contd.) : In computational simulations, a tension-dependent phosphorylation rate can explain tension-dependent detachment gradient.

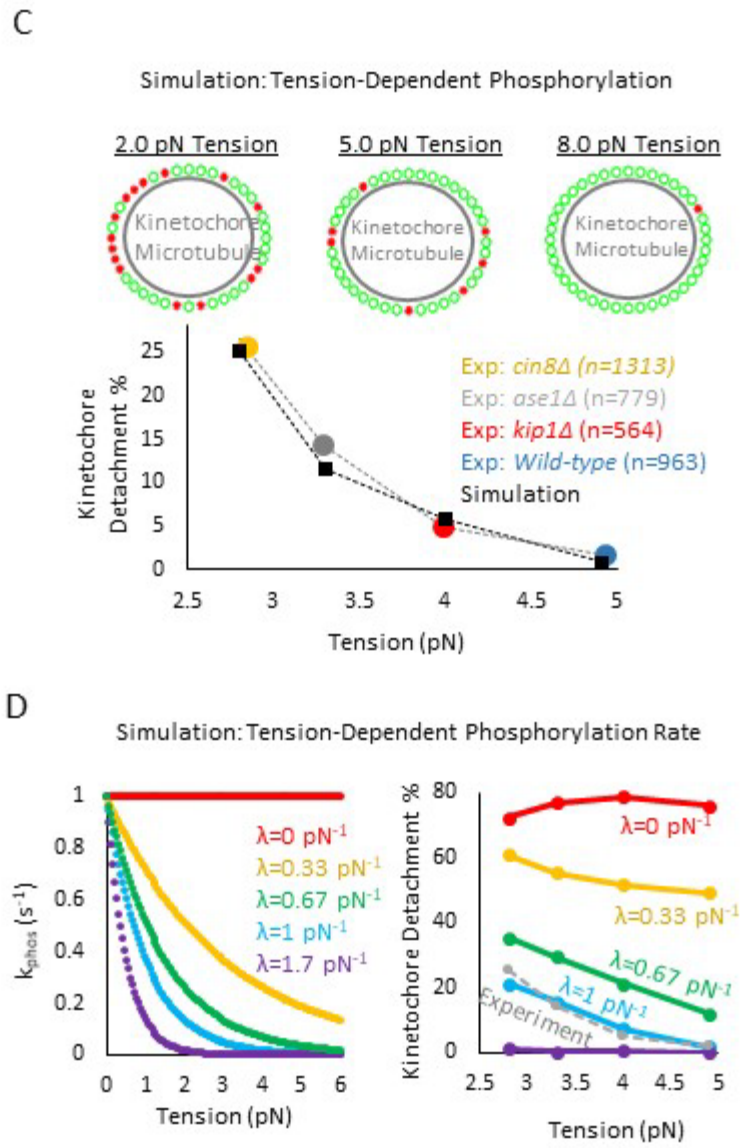

Figure 6 (contd.) : In computational simulations, a tension-dependent phosphorylation rate can explain tension-dependent detachment gradient.

Figure 6: In computational simulations, a tension-dependent phosphorylation rate can explain tension-dependent detachment gradient. (A) Speculative cartoon showing the architecture of a budding yeast kinetochore under high tension (left) and low tension (right). (B) The simulation tests whether a tension-dependent phosphorylation rate constant can explain our

experimentally observed gradient in detachment rates. Left: Schematic of simulation: each kinetochore has N_{sites} = 50 phosphorylation sites, which can stochastically switch between a phosphorylated state (red asterisks) and a dephosphorylated state (green circles). Right: The phosphorylation rate constant in the simulation is exponentially sensitive to tension (Eqn. 1), such that rapid phosphorylation occurs when tension is high, and slower phosphorylation occurs when tension is low. (C) Top: Representative images of the relationship between tension and the number of phosphorylated kinetochore sites in the simulation. Low tension leads to an increased number of phosphorylated sites on the kinetochore (left), while higher tension decreases the number of phosphorylated sites on the kinetochore (right) (see also Movie S1). Bottom: Plots showing the dependence of detachment rate on tension, as was experimentally observed (colored circles) and as predicted by simulation (black diamonds). The simulation can explain the observed gradient in detachment by using a tension-dependent phosphorylation rate as shown in Fig. 4B, right and Eqn. 1. (D) Left: λ was the scaling factor that determined the influence of tension on the phosphorylation rate constant (pN^{-1}) in Eqn. 1, such that for λ=0, there was no influence of tension on the phosphorylation rate constant (red), and for λ>0, increased tension would act to exponentially decrease the phosphorylation rate constant per Eqn. 1. Right: The best fit between experiment and simulation was for λ=1 pN^{-1} (light blue, experimental data shown as dotted grey line).

Chapter Seven: Proteomics based approaches directly demonstrate increased phosphorylation of kinetochore proteins in response to low tension.

Introduction

As previously discussed, the key process in cells initiating error correction in response to improperly oriented chromosomes is phosphorylation of proteins NDC80 and Dam1, which link the kinetochores to the microtubules. This allows erroneous connections to be turned over in favour of correctly oriented connections (Bloom and Yeh, 2010).

In this section we attempted to measure the abundance of the phosphorylated forms of these proteins relative to their unphosphorylated forms, and quantified how this ratio changed as a function of decreasing tension.

Previous work has shown that non-phoshphorylable mutants of Dam1 and NDC80 form hyper-stable connection that are not easily turned over, thus hampering error correction. Conversely, the kinetochore-microtubule connections in cells harboring phospho-mimetic versions of these proteins are weak, and these connections are easily severed. (Kemmler et al., 2009; Maresca and Salmon, 2010; Sarangapani et al., 2013; Tien et al., 2010; Wang et al., 2014).

It has also been shown that phosphorylation of NDC80 and Dam1 is gradually reduced as tension is slowly built up in the mitotic spindle as cells progress from prophase to metaphase (Keating et al., 2009)(Keating et al., 2009). However, direct, in vivo evidence of low tension leading to increased phosphorylation of NDC80 and Dam1 has never been put forward.

In this study we used both mass spectrometry, and western blot based approaches to demonstrate that Dam1 is increasingly phosphorylated as tension is lowered.

We focused our attention on Dam1 because it has been proposed that Dam1 is the more important target of Aurora B during error correction (Funabiki and Wynne, 2013). Phosphorylated Dam1 has altered electrophoretic mobility as compared to non-phosphorylated Dam1, and phosphorylation at multiple sites on Dam1 leads to a ladder of bands when this protein is run out on a Western blot. We took advantage of this effect to demonstrate increasing phosphorylation of Dam1 with decreasing tension.

The Aurora B phosphorylation sites on Dam1 have been well characterized. Dam1 has 4 sites which are phosphorylated by Aurora B, all of which were first identified from purified kinetochore sub-complexes (Cheeseman et al., 2002)using a mass spectrometry based exploration method (MacCoss et al., 2002). Later studies demonstrated that in-vitro phosphorylation of Dam1 reduced its affinity to microtubules, and three of the four sites on Dam1 were shown to play a key role in this process following in-vitro phosphorylation (Gestaut et al., 2008). Therefore, we selected one of these Dam1 phosphorylation sites, Serine 19, and used Multiple Reaction Monitoring (MRM) mass spectrometry to detect and quantify phosphorylation on Serine 19 of Dam1.

Results

Using a tension-dependent kinetochore phosphorylation rate constant (Eq. 4), our simulations predicted that we would observe an increasing gradient in kinetochore phosphorylation with decreasing tension (Fig. 7A). Since Dam1 is a key budding yeast kinetochore protein that is implicated in microtubule attachment (Joglekar et al., 2010) we then asked whether there was

an increasing gradient in Dam1 phosphorylation with decreasing tension, as was predicted by our simulations (Fig. 7A).

First, we leveraged the previously reported shift in electrophoretic mobility of phosphorylated Dam1 (Kang et al., 2001), to quantify the relative abundance of phosphorylated and de-phosphorylated forms of Dam1 in wild type cells, as well as in our three tension mutants. To validate this detection method, *cin8Δ* cells were arrested at metaphase by depletion of Cdc20, and 6-His-tagged Dam1 was purified from the *cin8Δ* cells using a nickel column. As expected, a western blot against the His tag showed a ladder of bands in the purified *cin8Δ* Dam1-His sample, which would be predicted to be highly phosphorylated (Fig. 7B, left). Importantly, this ladder collapsed down into a single band upon treatment with λ-phosphatase (Fig 7B, left), allowing us to establish a molecular weight cutoff between phosphorylated and dephosphorylated Dam1 protein (Fig. 7B, left, 55 kDa green line). This analysis is consistent with previously reported results (Kang et al., 2001), and suggests that the lowest band (below 55 kDa) represents the de-phosphorylated form of Dam1, while the upper bands (above 55 kDa) are progressively more phosphorylated. Quantification of relative band intensities within each of the lanes showed that untreated *cin8Δ* Dam1-His protein had multiple peaks over the range of 53 to 79 kDa, representing the observed ladder of bands (Fig. 5&, right, yellow), while the λ-phosphatase treated sample had only a single peak at ~54 kDa (Fig 7B, right, brown).

We then purified His tagged Dam1 protein from *Cdc20* metaphase-arrested wild-type and tension mutant cells, and ran the proteins from each strain in adjacent lanes on a single gel (Fig 7C left). Qualitatively, we observed an increasing shift towards the highest phosphorylation

level across the lanes (Fig. 7C, left, ~ 66 kDa). We then quantified the relative intensities within each respective lane (Fig. 7C, right). Similar to the control experiment (Fig. 7B), we observed an increasing number and relative intensity of peaks to the right of the 55 kDa cutoff for the tension mutants as compared to the wild-type cells (Fig. 7C, right). To compare the ratio of phosphorylated to dephosphorylated Dam1 in each case, we summed the total band intensity below 55 kDa (dephosphorylated Dam1), and above 55 kDa (phosphorylated Dam1), for each lane, and then plotted the ratio of phosphorylated to dephosphorylated Dam1 against average metaphase tension for each strain (Fig 7D, three replicate experiments shown). Strikingly, we observed an increasing gradient in the ratio of phosphorylated to dephosphorylated Dam1 with decreasing tension ($p=0.043$, single-factor ANOVA, 3 trials shown), similar to simulation predictions (Fig. 7D vs 7A).

Second, to increase the specificity of our western results, we measured the relative abundance of phosphorylated vs dephosphorylated Dam1 using tandem mass spectrometry.
For the mass spectrometry (MS) experiments, Dad1-Tap tagged protein was used to pull down unlabeled Dam1 protein from Cdc20 metaphase-arrested cells for all strains except *cin8Δ*, which was inviable in the presence of the Dad1-tap tag.(Shimogawa et al., 2006). To precisely quantify phosphorylation at Serine 19, the exact MS1 and MS2 spectra of the peptides LSIGSAPTSR and L(phosphoS)IGSAPTSR was first determined through creation of synthetic peptides and method development. The Combined Matrix Assisted Laser Desorption/Ionization (MALDI) spectra of crude synthetic peptide was collected, demonstrating mass to charge ratio (m/z) of 987.2342 (expected $[M+H]^+ = 987.114$) for the dephosphorylated Dam1 peptide LSIGSAPTSR and m/z of 1066.6511 (expected $[M+H]^+ = 1067.034$) for the phosphorylated Dam1

peptide L(Phospho-S)IGSAPTSR.(Fig 7E) Measurements were taken on a Bruker Autoflex MALDI mass spectrometer (Bremen, Germany). Upon HPLC purification both peptides were verified using liquid chromatography-tandem mass spectrometry (LC MS/MS) with prominent peaks representative of the expected Y4, Y5, Y6, Y7, Y8, and Y9 species detected in both the dephosphorylated and phosphorylated LSIGSAPTSR peptides. Measurements were taken on a SCIEX 5500 Qtrap Triple Quadrupole Mass Spectrometer (Framingham, MA)(Fig 7F).

Then, the quantities of the peptides L(phosphoS)IGSAPTSR and LSIGSAPTSR were measured using MRM (Fig. 7G, left, bottom). Similar to the western blot analysis for Dam1 as a whole, quantitative mass spectrometry demonstrated an increased phosphorylation ratio at Serine 19 of Dam1 with decreased tension (Fig. 5G, right; p=0.015, single-factor ANOVA, 3 groups).

Discussion

Phosphorylation of proteins comprising the load bearing components of the kinetochore-microtubule interface has been implicated as a key factor in initiation of error correction in response to low tension. However, these results have been based on the consequences of introducing phospho-mimetic or non-phosphorylable mutant versions of these proteins into cells being studies, and in-vitro results demonstrating the decreased affinity of phosphorylated forms of these proteins towards microtubules.

Here we present the first direct evidence that changes in tension directly affect the phospho-state of unmodified Dam1 in cells. We also show, using two separate methods, that the percentage of Dam1 that is phosphorylated increases with decreasing tension in a dose dependent manner. These results provide strong experimental support for the key rule we introduced into our simulations i.e phosphorylation frequency of kinetochore proteins increases

with decreasing tension. Taken together, these results provide a thorough mechanistic understanding of tension sensing, and how the tension sensing machinery can detect not just the presence or absence of tension, but is finely tuned to detect and respond to small changes in tension.

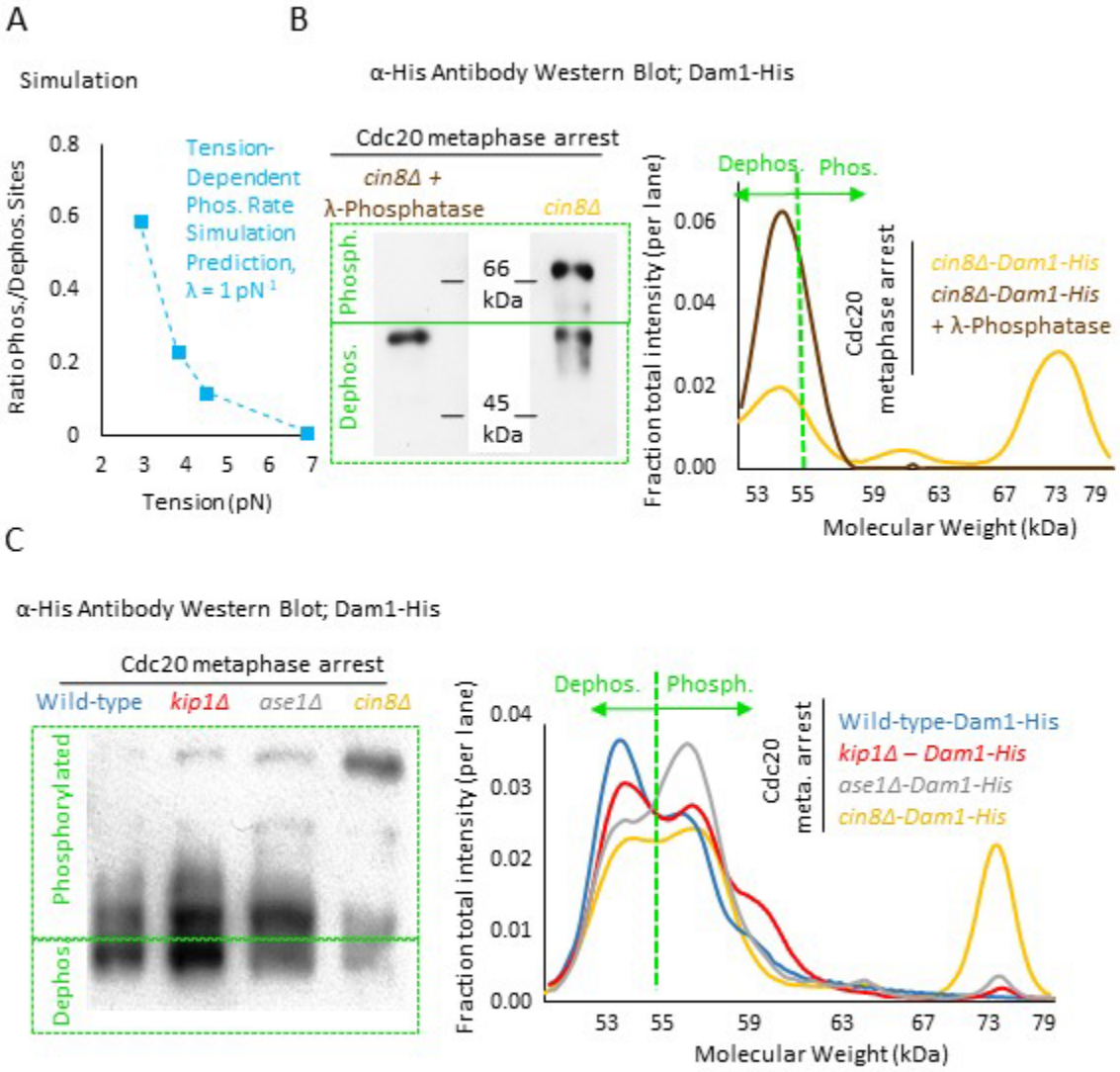

Figure 7 : A decreasing gradient in tension leads to an increasing gradient in Dam1 phosphorylation.

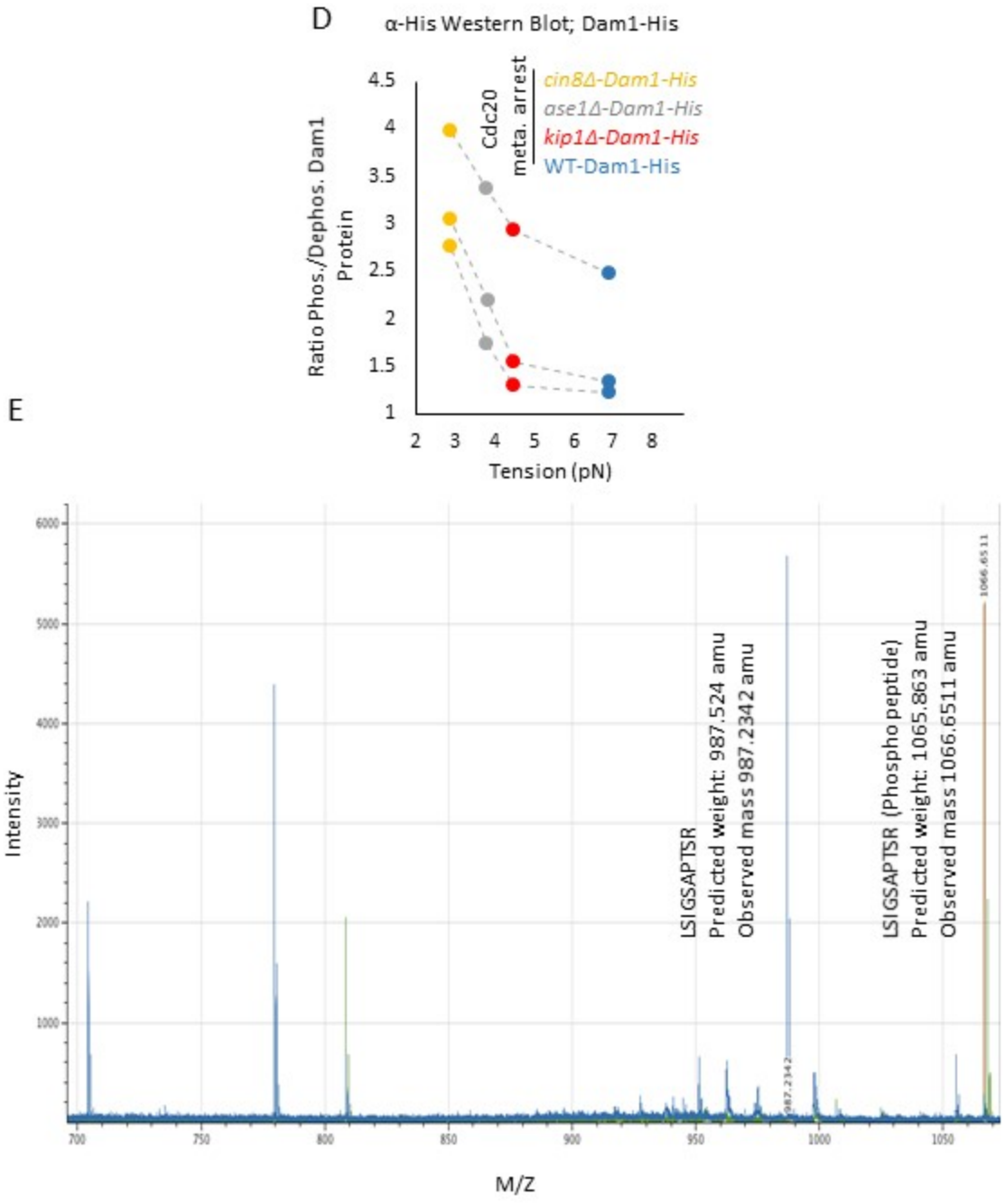

Figure 7 (contd.) : A decreasing gradient in tension leads to an increasing gradient in Dam1 phosphorylation.

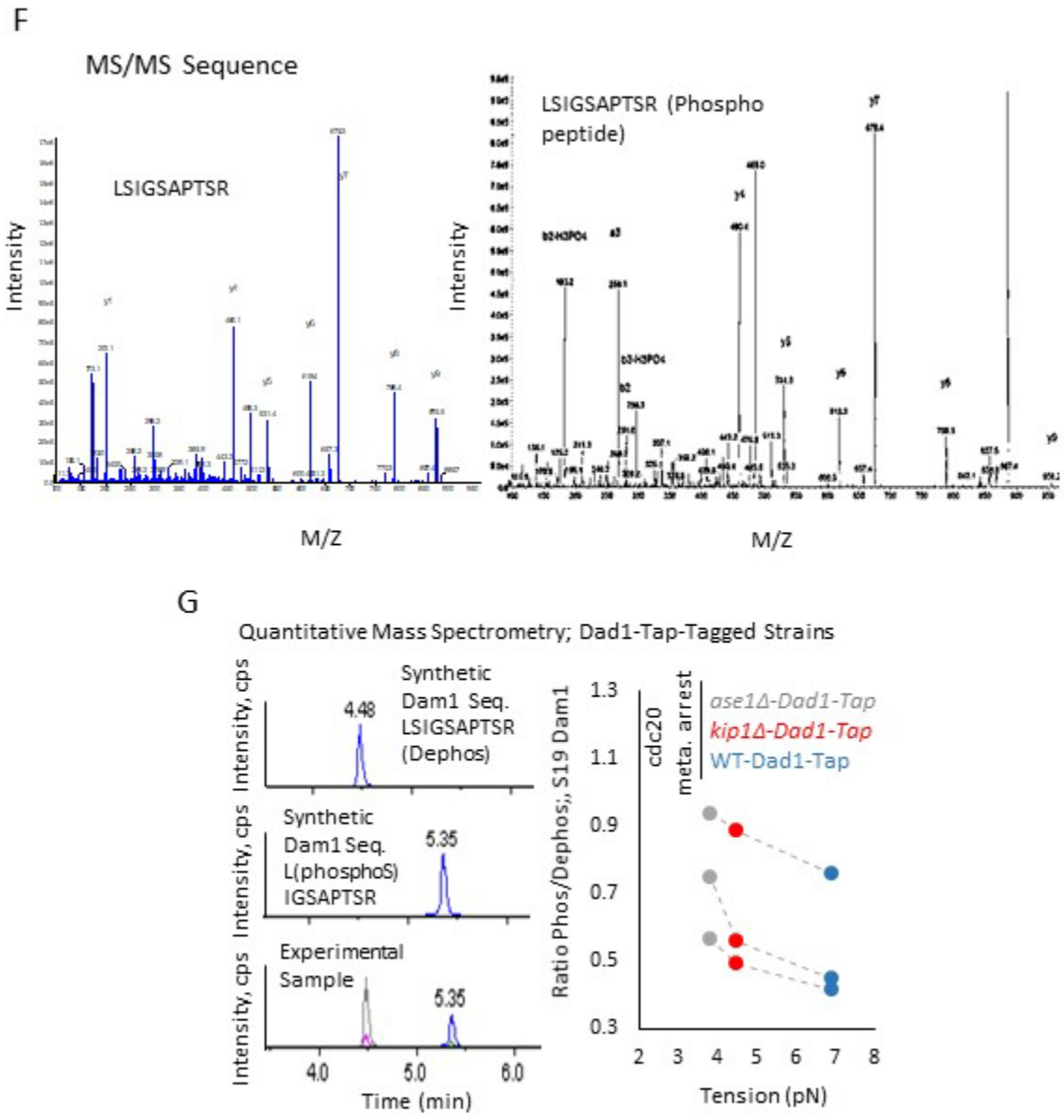

Figure 7 (contd.) : A decreasing gradient in tension leads to an increasing gradient in Dam1 phosphorylation.

Figure 7: A decreasing gradient in tension leads to an increasing gradient in Dam1 phosphorylation. (A) Simulation prediction for the ratio of phosphorylated kinetochore sites vs tension. (B) Left: Validation of anti-his western blot experiment to determine the effect of

phosphorylation on Dam1-his band locations in purified Cdc20-arrested *cin8Δ* Dam1-his proteins. Treatment of the *cin8Δ* Dam1-his proteins with λ-phosphatase collapses multiple bands down to one band at ~ 55 kDa. Right: Quantification of relative band intensities within the *cin8Δ* Dam1-his protein lane (yellow), and the lane with the *cin8Δ* Dam1-his protein treated with λ-phosphatase (brown). (C) Left: Anti-his western blots of Dam1-his purified from Cdc20-arrested wild-type and mutant cells. A shift towards higher molecular weights is indicative of increased phosphorylation. Right: Quantification of relative band intensities for each lane. (D) The ratio of phosphorylated (> 55 kDa) to dephosphorylated (≤ 55 kDa) Dam1 protein as calculated from western blot band intensities demonstrates increasing phosphorylation with decreasing tension (p=0.043, single-factor ANOVA, 3 individual trials shown).(E) Combined Matrix Assisted Laser Desorption/Ionization (MALDI) spectra of crude synthetic peptide demonstrating mass to charge ratio (m/z) of 987.2342 (expected $[M+H]^+$ = 987.114) for the dephosphorylated Dam1 peptide LSIGSAPTSR and m/z of 1066.6511 (expected $[M+H]^+$ = 1067.034) for the phosphorylated Dam1 peptide L(Phospho-S)IGSAPTSR.(F) HPLC purification of both peptides ,and verification using liquid chromatography-tandem mass spectrometry (LC MS/MS) with prominent peaks representative of the expected Y4, Y5, Y6, Y7, Y8, and Y9 species detected in both the dephosphorylated and phosphorylated LSIGSAPTSR peptides.(G) Left: Mass spectrometry scans of synthetic proteins (top and middle) and a typical experimental protein sample (bottom). Right: Quantitative mass spectrometry demonstrates an increasing gradient in the phosphorylation ratio at serine 19 of Dam1 with decreasing tension (3 individual trials shown, p=0.015, single-factor ANOVA, 3 groups).

Chapter Eight: Thesis Conclusions and Discussion

While tension has been long implicated to play a key role in allowing cells to sense errors in chromosomes orientation (Lampson and Cheeseman, 2011; Maresca and Salmon, 2010; Pinsky and Biggins, 2005), direct evidence to support this notion has never been put forward. Part of the reason tension has never been conclusively shown to play a role in error detection has been the fact there has been no good method to directly measure tension in live, unperturbed cells. Furthermore, attempts to reduce tension have altered microtubule dynamics or kinetochore structure in ways that make interpretation of the results difficult. In recent years, the debate surrounding the role of tension has taken a new turn, with some studies suggesting that errors in orientation are sensed because of the way these chromosomes are positioned on the mitotic spindle, rather than the tension they feel.

This study, based around an assay which allows for direct tension measurement, is the first one to unambiguously link low tension with downstream processes, such as detachment, that have previously been shown to play a key role in correcting erroneous kinetochore-microtubule connections.

In this study, we leveraged the balance of forces in the yeast mitotic spindle to generate a series of isogenic mutants that had a gradient in metaphase centromere tension. This allowed us to examine the role of tension during mitosis in spindles with robust microtubule dynamics and properly duplicated chromosomes. All of the tension mutants had significantly reduced centromere tension as compared to wild-type cells, and different mean tension values as compared to each other (Fig. 1C). In addition, the minimum observed mean tension (in *cin8Δ* cells,~2.8 pN) was still orders of magnitude larger than thermal forces (~0.01 pN), and so remained within range of forces that could act as a mechanical signal during mitosis. This

approach allowed us to ask whether cells would respond in a dose-dependent manner to moderate changes in the magnitude of tension. We found that the cellular response to tension was indeed dose-dependent in nature, such that the severity of the cellular response directly scaled with the average magnitude of metaphase tension. Thus, mitotic tension-sensing mechanisms within the cell are exquisitely sensitive. . While we used budding yeast as a model system for its simplified spindle structure and powerful genetics, we conjecture that this result is more relevant to other organisms. While budding yeast have a single microtubule attachment per kinetochore, the number of microtubules attachments per kinetochore ranges in nature from 2-3 in the fission yeast *S.pombe*, to 20-30 in mammalian and human systems. These systems raise the possibility, that of the multiple microtubules attaching to a given kinetochores, only a certain fraction would be erroneously attached. We expect that this would lead to a reduction in tension, rather than a complete absence of tension, and a cell would be aided by a system like the one we describe, which is able to sense small changes in tension and mount a commensurate response. As the core tension sensing machinery is largely conserved from budding yeast to humans (Biggins et al., 1999; Cheeseman et al., 2006; Joglekar et al., 2008), we believe that the general principles discovered in yeast also apply to higher eukaryotes. Interesting future work could center around testing this hypothesis experimentally using cell lines derived from more advanced eukaryotic species.

Our observation of increasing detachment rates with decreasing tension magnitudes strongly suggests that error detection and tension sensing are part of the same pathway. We also demonstrated that the generation of kinetochore detachments in response to low tension was dependent on the activity of Aurora B, a protein known to play a crucial role in turnover of

improper kinetochore-microtubule attachments (Hauf et al., 2003; Kapoor et al., 2000; Tanaka et al., 2002). Recent data has shown than the primary role of Aurora B during error correction in meiosis I is the creation of detachments, especially on chromosomes that show reduced inter-kinetochore distances, and that Spindle Assembly Checkpoint activation occurs downstream of this in an Aurora B independent manner(Vallot et al., 2017) . Our data strongly supports the notion that a similar process operates in mitosis, and builds on this model to demonstrate that this process is directly dependent on tension sensing and is tuned such that the cellular response scales with tension in an exquisitely dose dependent manner.

We used computational modeling to investigate a potential mechanism to explain our experimentally observed dose-dependent response to low tension, which also provides directions for future explorations. We found that our probabilistic model could faithfully recapitulate our experimental observations of a dose-dependent detachment response to decreasing average tension magnitudes if (1) the kinetochore phosphorylation rate was tension dependent, and (2) the strength of the kinetochore-microtubule binding interface was directly reduced by an increasing fraction of phosphorylated sites. Interesting future work will involve testing these assumptions, for example, by predicting and experimentally evaluating changes to the tension-dependent detachment rate gradient in mutants with altered numbers of active kinetochore phosphorylation sites (Akiyoshi et al., 2009a; Sarangapani et al., 2013; Tien et al., 2010). In addition, the underlying physical mechanism of a tension-dependent kinetochore phosphorylation rate may involve the kinetochore itself stretching under high tension (Maresca and Salmon, 2010), and limiting the accessibility of Aurora B to its substrates (Fig 4A) (Liu et al., 2009; Maresca and Salmon, 2009), but this particular mechanism remains controversial

(Dumont et al., 2012) (Magidson et al., 2016). However, as our proteomics work shows, low tension is associated with increased phosphorylation of kinetochore associated proteins known to play a key role in modulation kinetochore-microtubule attachment. Therefore, it is clear that tension sensing involves phosphorylation of the outer kinetochore in order to detach microtubule connections that are likely to be erroneous, even as the finer details of how low tension is translated into high phosphorylation continues to be a subject of debate. Thus, interesting future work could also center on the origin of a tension-dependent phosphorylation rate constant, since we predict that alterations in component(s) that mediate a tension-dependent kinetochore phosphorylation rate would directly alter our experimentally observed gradient in detachment rate as a function of tension.

In this work we concentrated on the phosphorylation of a single protein target of Aurora B , Dam1. Future work focusing on measuring tension dependent phosphorylation of NDC80, along with other kinetochore components might prove to be extremely informative in building up a more mechanistic understanding of cellular responses, especially checkpoint signaling, downstream of tension sensing.

Overall, our results allow us to start building a model of how low tension is sensed in the cell and translated to a downstream response to correct orientation defects which lead to low tension. The first response of the cell to low tension is to create detached kinetochores. Detached kinetochores are sensed by the spindle assembly checkpoint, which delays cells in metaphase until the kinetochores can be re-attached using a stochastic search and capture process. Failure of the Spindle Assembly Checkpoint to sense detachments allows cells to enter anaphase with unattached chromosomes, which are mis-segregated. Therefore, tension sensing

allows cells to turn-over erroneous kinetochore-microtubule attachments, while ensuring anaphase does not commence until proper connections have been re-established.

References

Akiyoshi, B., Nelson, C.R., Ranish, J. a., and Biggins, S. (2009a). Analysis of Ipl1-mediated phosphorylation of the Ndc80 kinetochore protein in Saccharomyces cerevisiae. Genetics *183*, 1591–1595.

Akiyoshi, B., Nelson, C.R., Ranish, J.A., and Biggins, S. (2009b). Quantitative proteomic analysis of purified yeast kinetochores identifies a PP1 regulatory subunit. Genes Dev. *23*, 2887–2899.

Akiyoshi, B., Sarangapani, K.K., Powers, A.F., Nelson, C.R., Reichow, S.L., Arellano-Santoyo, H., Gonen, T., Ranish, J. a, Asbury, C.L., and Biggins, S. (2010). Tension directly stabilizes reconstituted kinetochore-microtubule attachments. Nature *468*, 576–579.

Asbury, C.L., Gestaut, D.R., Powers, A.F., Franck, A.D., and Davis, T.N. (2006). The Dam1 kinetochore complex harnesses microtubule dynamics to produce force and movement. Proc. Natl. Acad. Sci. U. S. A. *103*, 9873–9878.

Biggins, S., and Murray, a W. (2001). The budding yeast protein kinase Ipl1/Aurora allows the absence of tension to activate the spindle checkpoint. Genes Dev. *15*, 3118–3129.

Biggins, S., Severin, F., and Bhalla, N. (1999). The conserved protein kinase Ipl1 regulates microtubule binding to kinetochores in budding yeast. Genes … 532–544.

Bloom, K., and Yeh, E. (2010). Tension management in the kinetochore. Curr. Biol. *20*, R1040-8.

Chacon, J.M., Mukherjee, S., Schuster, B.M., Clarke, D.J., and Gardner, M.K. (2014). Pericentromere tension is self-regulated by spindle structure in metaphase. J. Cell Biol. *205*, 313–324.

Chao, W.C.H., Kulkarni, K., Zhang, Z., Kong, E.H., and Barford, D. (2012). Structure of the mitotic

checkpoint complex. Nature *484*, 208–213.

Cheeseman, I.M., Brew, C., Wolyniak, M., Desai, A., Anderson, S., Muster, N., Yates, J.R., Huffaker, T.C., Drubin, D.G., and Barnes, G. (2001). Implication of a novel multiprotein Dam1p complex in outer kinetochore function. J. Cell Biol. *155*, 1137–1145.

Cheeseman, I.M., Anderson, S., Jwa, M., Green, E.M., Kang, J.S., Yates, J.R., Chan, C.S.M., Drubin, D.G., and Barnes, G. (2002). Phospho-regulation of kinetochore-microtubule attachments by the Aurora kinase Ipl1p. Cell *111*, 163–172.

Cheeseman, I.M., Chappie, J.S., Wilson-Kubalek, E.M., and Desai, A. (2006). The conserved KMN network constitutes the core microtubule-binding site of the kinetochore. Cell *127*, 983–997.

Chmátal, L., Yang, K., Schultz, R.M., and Lampson, M.A. (2015). Spatial Regulation of Kinetochore Microtubule Attachments by Destabilization at Spindle Poles in Meiosis I. Curr. Biol. *25*, 1835–1841.

Cimini, D., Wan, X., Hirel, C.B., and Salmon, E.D. (2006). Aurora kinase promotes turnover of kinetochore microtubules to reduce chromosome segregation errors. Curr. Biol. *16*, 1711–1718.

Cohen-Fix, O., and Koshland, D. (1997). The metaphase-to-anaphase transition: Avoiding a mid-life crisis. Curr. Opin. Cell Biol. *9*, 800–806.

Collin, P., Nashchekina, O., Walker, R., and Pines, J. (2013). The spindle assembly checkpoint works like a rheostat rather than a toggle switch. Nat. Cell Biol. *15*, 1378–1385.

Dick, A.E., and Gerlich, D.W. (2013). Kinetic framework of spindle assembly checkpoint signalling. Nat. Cell Biol. *15*, 1370–1377.

Dumont, S., Salmon, E.D., and Mitchison, T.J. (2012). Deformations within moving kinetochores reveal different sites of active and passive force generation. Science *337*, 355–358.

Elledge, S. (1996). Cell cycle checkpoints: preventing an identity crisis. Science (80-.). *274*, 1664–1672.

Elowe, S., Hümmer, S., Uldschmid, A., Li, X., and Nigg, E. a (2007). Tension-sensitive Plk1 phosphorylation on BubR1 regulates the stability of kinetochore microtubule interactions. Genes Dev. *21*, 2205–2219.

Funabiki, H., and Wynne, D.J. (2013). Making an effective switch at the kinetochore by phosphorylation and dephosphorylation. Chromosoma *122*, 135–158.

Gardner, M.K., Bouck, D.C., Paliulis, L. V, Meehl, J.B., O'Toole, E.T., Haase, J., Soubry, A., Joglekar, A.P., Winey, M., Salmon, E.D., et al. (2008). Chromosome congression by Kinesin-5 motor-mediated disassembly of longer kinetochore microtubules. Cell *135*, 894–906.

Gatlin, J.C., and Bloom, K. (2010). Microtubule motors in eukaryotic spindle assembly and maintenance. Semin. Cell Dev. Biol. *21*, 248–254.

Gestaut, D.R., Graczyk, B., Cooper, J., Widlund, P.O., Zelter, A., Wordeman, L., Asbury, C.L., and Davis, T.N. (2008). Phosphoregulation and depolymerization-driven movement of the Dam1 complex do not require ring formation. Nat. Cell Biol. *10*, 407–414.

Griffis, E.R., Stuurman, N., and Vale, R.D. (2007). Spindly, a novel protein essential for silencing the spindle assembly checkpoint, recruits dynein to the kinetochore. J. Cell Biol. *177*, 1005–1015.

Grishchuk, E.L., Molodtsov, M.I., Ataullakhanov, F.I., and McIntosh, J.R. (2005). Force production by disassembling microtubules. Nature *438*, 384–388.

Haase, J., Bonner, M.K., Halas, H., and Kelly, A.E. (2017). Distinct Roles of the Chromosomal Passenger Complex in the Detection of and Response to Errors in Kinetochore-Microtubule Attachment. Dev. Cell *42*, 640–654.e5.

Han, J.S., Holland, A.J., Fachinetti, D., Kulukian, A., Cetin, B., and Cleveland, D.W. (2013). Catalytic assembly of the mitotic checkpoint inhibitor BubR1-Cdc20 by a Mad2-induced functional Switch in Cdc20. Mol. Cell *51*, 92–104.

Hauf, S., Cole, R., and LaTerra, S. (2003). The small molecule Hesperadin reveals a role for Aurora B in correcting kinetochore–microtubule attachment and in maintaining the spindle assembly checkpoint. J. Cell … 281–294.

Hepperla, A.J., Willey, P.T., Coombes, C.E., Schuster, B.M., Gerami-Nejad, M., McClellan, M., Mukherjee, S., Fox, J., Winey, M., Odde, D.J., et al. (2014). Minus-End-Directed Kinesin-14 Motors Align Antiparallel Microtubules to Control Metaphase Spindle Length. Dev. Cell *31*, 61–72.

Hildebrandt, E.R., and Hoyt, M. a (2000). Mitotic motors in Saccharomyces cerevisiae. Biochim. Biophys. Acta *1496*, 99–116.

Hirano, T. (2006). At the heart of the chromosome: SMC proteins in action. Nat. Rev. Mol. Cell Biol. *7*, 311–322.

Itabashi, T., Terada, Y., Kuwana, K., Kan, T., Shimoyama, I., and Ishiwata, S. (2012). Mechanical impulses can control metaphase progression in a mammalian cell. Proc. Natl. Acad. Sci. U. S. A. *109*, 7320–7325.

Janson, M.E., Loughlin, R., Loïodice, I., Fu, C., Brunner, D., Nédélec, F.J., and Tran, P.T. (2007). Crosslinkers and Motors Organize Dynamic Microtubules to Form Stable Bipolar Arrays in Fission Yeast. Cell *128*, 357–368.

Jaqaman, K., King, E.M., Amaro, A.C., Winter, J.R., Dorn, J.F., Elliott, H.L., Mchedlishvili, N., McClelland, S.E., Porter, I.M., Posch, M., et al. (2010). Kinetochore alignment within the metaphase plate is regulated by centromere stiffness and microtubule depolymerases. J. Cell Biol. *188*, 665–679.

Jin, F., Liu, H., Li, P., Yu, H.-G., and Wang, Y. (2012). Loss of function of the Cik1/Kar3 motor complex results in chromosomes with syntelic attachment that are sensed by the tension checkpoint. PLoS Genet. *8*, e1002492.

Joglekar, A. (2016). A Cell Biological Perspective on Past, Present and Future Investigations of the Spindle Assembly Checkpoint. Biology (Basel). *5*, 44.

Joglekar, A.P., Bouck, D.C., Molk, J.N., Bloom, K.S., and Salmon, E.D. (2006). Molecular architecture of a kinetochore-microtubule attachment site. Nat. Cell Biol. *8*, 581–585.

Joglekar, A.P., Bouck, D., Finley, K., Liu, X., Wan, Y., Berman, J., He, X., Salmon, E.D., and Bloom, K.S. (2008). Molecular architecture of the kinetochore-microtubule attachment site is conserved between point and regional centromeres. J. Cell Biol. *181*, 587–594.

Joglekar, A.P., Bloom, K.S., and Salmon, E.D. (2010). Mechanisms of force generation by end-on kinetochore-microtubule attachments. Curr. Opin. Cell Biol. *22*, 57–67.

Juang, Y.L., Huang, J., Peters, J.M., McLaughlin, M.E., Tai, C.Y., and Pellman, D. (1997). APC-mediated proteolysis of Ase1 and the morphogenesis of the mitotic spindle. Science *275*, 1311–1314.

Kalinina, I., Nandi, A., Delivani, P., Chacón, M.R., Klemm, A.H., Ramunno-Johnson, D., Krull, A., Lindner, B., Pavin, N., and Tolić-Nørrelykke, I.M. (2013). Pivoting of microtubules around the spindle pole accelerates kinetochore capture. Nat. Cell Biol. *15*, 82–87.

Kallio, M.J., McCleland, M.L., Stukenberg, P.T., and Gorbsky, G.J. (2002). Inhibition of aurora B kinase blocks chromosome segregation, overrides the spindle checkpoint, and perturbs microtubule dynamics in mitosis. Curr. Biol. *12*, 900–905.

Kang, J.S., Cheeseman, I.M., Kallstrom, G., Velmurugan, S., Barnes, G., and Chan, C.S.M. (2001). Functional cooperation of Dam1, Ipl1, and the inner centromere protein (INCENP)-related protein Sli15 during chromosome segregation. J. Cell Biol. *155*, 763–774.

Kapoor, T.M., Mayer, T.U., Coughlin, M.L., and Mitchison, T.J. (2000). Probing spindle assembly mechanisms with monastrol, a small molecule inhibitor of the mitotic kinesin, Eg5. J. Cell Biol. *150*, 975–988.

Keating, P., Rachidi, N., Tanaka, T.U., and Stark, M.J.R. (2009). Ipl1-dependent phosphorylation of Dam1 is reduced by tension applied on kinetochores. J. Cell Sci. *122*, 4375–4382.

Kelly, A.E., and Funabiki, H. (2009). Correcting aberrant kinetochore microtubule attachments: an Aurora B-centric view. Curr. Opin. Cell Biol. *21*, 51–58.

Kemmler, S., Stach, M., Knapp, M., Ortiz, J., Pfannstiel, J., Ruppert, T., and Lechner, J. (2009). Mimicking Ndc80 phosphorylation triggers spindle assembly checkpoint signalling. EMBO J. *28*, 1099–1110.

Khodjakov, A., and Pines, J. (2010). Centromere tension: a divisive issue. Nat Cell Biol *12*, 919–923.

King, J.M., and Nicklas, R.B. (2000). Tension on chromosomes increases the number of kinetochore microtubules but only within limits. J. Cell Sci. *113 Pt 21*, 3815–3823.

Kops, G.J.P.L., Weaver, B. a a, and Cleveland, D.W. (2005). On the road to cancer: aneuploidy and the mitotic checkpoint. Nat. Rev. Cancer *5*, 773–785.

Kotwaliwale, C. V., Frei, S.B., Stern, B.M., and Biggins, S. (2007). A Pathway Containing the Ipl1/Aurora Protein Kinase and the Spindle Midzone Protein Ase1 Regulates Yeast Spindle Assembly. Dev. Cell *13*, 433–445.

Lampert, F., and Westermann, S. (2011). A blueprint for kinetochores - new insights into the molecular mechanics of cell division. Nat. Rev. Mol. Cell Biol. *12*, 407–412.

Lampson, M. a, and Cheeseman, I.M. (2011). Sensing centromere tension: Aurora B and the regulation of kinetochore function. Trends Cell Biol. *21*, 133–140.

Lampson, M. a, Renduchitala, K., Khodjakov, A., and Kapoor, T.M. (2004). Correcting improper chromosome-spindle attachments during cell division. Nat. Cell Biol. *6*, 232–237.

Lesage, B., Qian, J., and Bollen, M. (2011). Spindle checkpoint silencing: PP1 tips the balance. Curr. Biol. *21*, R898–R903.

Lew, D.J., and Burke, D.J. (2003). The spindle assembly and spindle position checkpoints. Annu. Rev. Genet. *37*, 251–282.

Li, X., and Nicklas, R.B. (1997). Tension-sensitive kinetochore phosphorylation and the chromosome distribution checkpoint in praying mantid spermatocytes. J. Cell Sci. *110 (Pt 5*, 537–545.

Liu, D., Vader, G., Vromans, M.J.M., Lampson, M.A., and Lens, S.M.A. (2009). Sensing chromosome bi-orientation by spatial separation of aurora B kinase from kinetochore substrates. Science *323*, 1350–1353.

Liu, D., Davydenko, O., and Lampson, M. a (2012). Polo-like kinase-1 regulates kinetochore-microtubule dynamics and spindle checkpoint silencing. J. Cell Biol. *198*, 491–499.

Liu, H., Liang, F., Jin, F., and Wang, Y. (2008). The coordination of centromere replication, spindle formation, and kinetochore-microtubule interaction in budding yeast. PLoS Genet. *4*.

Lu, D., Hsiao, J.Y., Davey, N.E., Van Voorhis, V. a., Foster, S. a., Tang, C., and Morgan, D.O. (2014). Multiple mechanisms determine the order of APC/C substrate degradation in mitosis. J. Cell Biol. *207*.

MacCoss, M.J., McDonald, W.H., Saraf, A., Sadygov, R., Clark, J.M., Tasto, J.J., Gould, K.L., Wolters, D., Washburn, M., Weiss, A., et al. (2002). Shotgun identification of protein modifications from protein complexes and lens tissue. Proc. Natl. Acad. Sci. U. S. A. *99*, 7900–7905.

Magidson, V., Paul, R., Yang, N., Ault, J.G., O'Connell, C.B., Tikhonenko, I., McEwen, B.F., Mogilner, A., and Khodjakov, A. (2015). Adaptive changes in the kinetochore architecture facilitate proper spindle assembly. Nat. Cell Biol. *17*, 1134–1144.

Magidson, V., He, J., Ault, J.G., Connell, C.B.O., Yang, N., Tikhonenko, I., Mcewen, B.F., Sui, H., and Khodjakov, A. (2016). Unattached kinetochores rather than intrakinetochore tension arrest mitosis in taxol-treated cells. J. Cell Biol. *212*, 307–319.

Marco, E., Dorn, J.F., Hsu, P., Jaqaman, K., Sorger, P.K., and Danuser, G. (2013). S. cerevisiae chromosomes biorient via gradual resolution of syntely between S phase and anaphase. Cell *154*, 1127–1139.

Maresca, T.J., and Salmon, E.D. (2009). Intrakinetochore stretch is associated with changes in kinetochore

phosphorylation and spindle assembly checkpoint activity. J. Cell Biol. *184*, 373–381.

Maresca, T.J., and Salmon, E.D. (2010). Welcome to a new kind of tension: translating kinetochore mechanics into a wait-anaphase signal. J. Cell Sci. *123*, 825–835.

Miller, M.P., Asbury, C.L., and Biggins, S. (2016). A TOG protein confers tension sensitivity to kinetochore-microtubule attachments. Cell *165*, 1428–1439.

Moyle, M.W., Kim, T., Hattersley, N., Espeut, J., Cheerambathur, D.K., Oegema, K., and Desai, A. (2014). A Bub1-Mad1 interaction targets the Mad1-Mad2 complex to unattached kinetochores to initiate the spindle checkpoint. J. Cell Biol. *204*, 647–657.

Muñoz-Barrera, M., and Monje-Casas, F. (2014). Increased Aurora B activity causes continuous disruption of kinetochore-microtubule attachments and spindle instability. Proc. Natl. Acad. Sci. U. S. A.

Musacchio, A., and Salmon, E.D. (2007). The spindle-assembly checkpoint in space and time. Nat. Rev. Mol. Cell Biol. *8*, 379–393.

Nezi, L., and Musacchio, A. (2009). Sister chromatid tension and the spindle assembly checkpoint. Curr. Opin. Cell Biol. *21*, 785–795.

Nicklas, R.B. (1997). How cells get the right chromosomes. Science *275*, 632–637.

Nicklas, R.B., and Koch, C.A. (1969). Chromosome micromanipulation. 3. Spindle fiber tension and the reorientation of mal-oriented chromosomes. J. Cell Biol. *43*, 40–50.

Nicklas, R.B., Waters, J.C., Salmon, E.D., and Ward, S.C. (2001). Checkpoint signals in grasshopper meiosis are sensitive to microtubule attachment, but tension is still essential. J. Cell Sci. *114*, 4173–4183.

O'Connell, C.B., Loncarek, J., Hergert, P., Kourtidis, A., Conklin, D.S., and Khodjakov, A. (2008). The spindle assembly checkpoint is satisfied in the absence of interkinetochore tension during mitosis with unreplicated genomes. J. Cell Biol. *183*, 29–36.

O'Toole, E.T., Winey, M., and McIntosh, J.R. (1999). High-voltage electron tomography of spindle pole bodies and early mitotic spindles in the yeast Saccharomyces cerevisiae. Mol. Biol. Cell *10*, 2017–2031.

Pearson, C.G., Maddox, P.S., Salmon, E.D., and Bloom, K. (2001). Budding Yeast Chromosome Structure and Dynamics during Mitosis. J. Cell Biol. *152*, 1255–1266.

Pinsky, B. a, and Biggins, S. (2005). The spindle checkpoint: tension versus attachment. Trends Cell Biol. *15*, 486–493.

Pinsky, B. a, Kung, C., Shokat, K.M., and Biggins, S. (2006). The Ipl1-Aurora protein kinase activates the spindle checkpoint by creating unattached kinetochores. Nat. Cell Biol. *8*, 78–83.

Pinsky, B. a, Nelson, C.R., and Biggins, S. (2009). Protein phosphatase 1 regulates exit from the spindle checkpoint in budding yeast. Curr. Biol. *19*, 1182–1187.

Powers, A.F., Franck, A.D., Gestaut, D.R., Cooper, J., Gracyzk, B., Wei, R.R., Wordeman, L., Davis, T.N., and Asbury, C.L. (2009). The Ndc80 kinetochore complex forms load-bearing attachments to dynamic microtubule tips via biased diffusion. Cell *136*, 865–875.

Rizk, R.S., Bohannon, K.P., Wetzel, L.A., Powers, J., Shaw, S.L., and Walczak, C.E. (2009). MCAK and Paclitaxel Have Differential Effects on Spindle Microtubule Organization and Dynamics. Mol. Biol. Cell *20*, 1639–1651.

Salmon, E.D., and Bloom, K. (2017). Tension sensors reveal how the kinetochore shares its load. BioEssays *39*, 1–11.

Sarangapani, K.K., Akiyoshi, B., Duggan, N.M., Biggins, S., and Asbury, C.L. (2013). Phosphoregulation promotes release of kinetochores from dynamic microtubules via multiple mechanisms. Proc. Natl. Acad. Sci. U. S. A. *110*, 7282–7287.

Schuyler, S.C., Liu, J.Y., and Pellman, D. (2003). The molecular function of Ase1p: Evidence for a MAP-

dependent midzone-specific spindle matrix. J. Cell Biol. *160*, 517–528.

Shimogawa, M.M., Graczyk, B., Gardner, M.K., Francis, S.E., White, E.A., Ess, M., Molk, J.N., Ruse, C., Niessen, S., Yates, J.R., et al. (2006). Mps1 Phosphorylation of Dam1 Couples Kinetochores to Microtubule Plus Ends at Metaphase. Curr. Biol. *16*, 1489–1501.

Shimogawa, M.M., Wargacki, M.M., Muller, E.G., and Davis, T.N. (2010). Laterally attached kinetochores recruit the checkpoint protein Bub1, but satisfy the spindle checkpoint. Cell Cycle *9*, 3619–3628.

Stephens, A.D., Haase, J., Vicci, L., Taylor, R.M., and Bloom, K. (2011). Cohesin, condensin, and the intramolecular centromere loop together generate the mitotic chromatin spring. J. Cell Biol. *193*, 1167–1180.

Stern, B.M., and Murray, a W. (2001). Lack of tension at kinetochores activates the spindle checkpoint in budding yeast. Curr. Biol. *11*, 1462–1467.

Straight, A.F., Sedat, J.W., and Murray, A.W. (1998). Time-lapse microscopy reveals unique roles for kinesins during anaphase in budding yeast. J. Cell Biol. *143*, 687–694.

Suzuki, A., Hori, T., Nishino, T., Usukura, J., Miyagi, A., Morikawa, K., and Fukagawa, T. (2011). Spindle microtubules generate tension-dependent changes in the distribution of inner kinetochore proteins. J. Cell Biol. *193*, 125–140.

Suzuki, A., Badger, B.L., Wan, X., DeLuca, J.G., and Salmon, E.D. (2014). The Architecture of CCAN Proteins Creates a Structural Integrity to Resist Spindle Forces and Achieve Proper Intrakinetochore Stretch. Dev. Cell *30*, 717–730.

Tanaka, T.U., Rachidi, N., Janke, C., Pereira, G., Galova, M., Schiebel, E., Stark, M.J.R., and Nasmyth, K. (2002). Evidence that the Ipl1-Sli15 (Aurora kinase-INCENP) complex promotes chromosome bi-orientation by altering kinetochore-spindle pole connections. Cell *108*, 317–329.

Tien, J.F., Umbreit, N.T., Gestaut, D.R., Franck, A.D., Cooper, J., Wordeman, L., Gonen, T., Asbury, C.L., and Davis, T.N. (2010). Cooperation of the Dam1 and Ndc80 kinetochore complexes enhances microtubule coupling and is regulated by aurora B. J. Cell Biol. *189*, 713–723.

Vallot, A., Leontiou, I., Cladière, D., El Yakoubi, W., Bolte, S., Buffin, E., and Wassmann, K. (2017). Tension-Induced Error Correction and Not Kinetochore Attachment Status Activates the SAC in an Aurora-B/C-Dependent Manner in Oocytes. Curr. Biol. 130–139.

Varma, D., Wan, X., Cheerambathur, D., Gassmann, R., Suzuki, A., Lawrimore, J., Desai, A., and Salmon, E.D. (2013). Spindle assembly checkpoint proteins are positioned close to core microtubule attachment sites at kinetochores. J. Cell Biol. *202*, 735–746.

Vigneron, S., Prieto, S., and Bernis, C. (2004). Kinetochore localization of spindle checkpoint proteins: who controls whom? Mol. Biol. … *15*, 4584–4596.

Walczak, C.E., and Heald, R. (2008). Mechanisms of mitotic spindle assembly and function. Int. Rev. Cytol. *265*, 111–158.

Wan, X., and Cimini, D. (2012). The coupling between sister kinetochore directional instability and oscillations in centromere stretch in metaphase PtK1 cells. Mol. Biol. … *23*.

Wan, X., O'Quinn, R.P., Pierce, H.L., Joglekar, A.P., Gall, W.E., DeLuca, J.G., Carroll, C.W., Liu, S.-T., Yen, T.J., McEwen, B.F., et al. (2009). Protein architecture of the human kinetochore microtubule attachment site. Cell *137*, 672–684.

Wang, Y., Jin, F., Higgins, R., and McKnight, K. (2014). The current view for the silencing of the spindle assembly checkpoint. Cell Cycle *13*, 1694–1701.

Wargacki, M.M., Tay, J.C., Muller, E.G., Asbury, C.L., and Davis, T.N. (2010). Kip3, the yeast kinesin-8, is required for clustering of kinetochores at metaphase. Cell Cycle *9*, 2581–2588.

Waters, J.C., Chen, R.H., Murray, a W., and Salmon, E.D. (1998). Localization of Mad2 to kinetochores depends on microtubule attachment, not tension. J. Cell Biol. *141*, 1181–1191.

Welburn, J.P.I., Vleugel, M., Liu, D., Yates, J.R., Lampson, M. a, Fukagawa, T., and Cheeseman, I.M. (2010). Aurora B phosphorylates spatially distinct targets to differentially regulate the kinetochore-microtubule interface. Mol. Cell *38*, 383–392.

Westermann, S., Drubin, D.G., and Barnes, G. (2007). Structures and functions of yeast kinetochore complexes. Annu. Rev. Biochem. *76*, 563–591.

Wurzenberger, C., and Gerlich, D.W. (2011). Phosphatases: providing safe passage through mitotic exit. Nat. Rev. Mol. Cell Biol. *12*, 469–482.

Yamagishi, Y., Sakuno, T., Goto, Y., and Watanabe, Y. (2014). Kinetochore composition and its function: lessons from yeasts. FEMS Microbiol. Rev. *38*, 185–200.

Yang, Z., Kenny, A.E., Brito, D. a, and Rieder, C.L. (2009). Cells satisfy the mitotic checkpoint in Taxol, and do so faster in concentrations that stabilize syntelic attachments. J. Cell Biol. *186*, 675–684.

Ye, A.A., Deretic, J., Hoel, C.M., Hinman, A.W., Cimini, D., Welburn, J.P., and Maresca, T.J. (2015). Aurora A Kinase Contributes to a Pole-Based Error Correction Pathway. Curr. Biol. *25*, 1842–1851.

Zaytsev, a. V., Mick, J.E., Maslennikov, E., Nikashin, B., DeLuca, J.G., and Grishchuk, E.L. (2015). Multisite phosphorylation of the NDC80 complex gradually tunes its microtubule-binding affinity. Mol. Biol. Cell *26*, 1829–1844.

Appendix A : Materials and Methods

In vivo imaging of *S. Cerevisiae* mitotic spindles

A list of yeast strains is given in Table 3. Cells were imaged on a TIRF microscope (Nikon Eclipse Ti) using 405 nm, 488 nm and 561 nm laser lines. Yeast cells were adhered to a cover slip and then imaged using a pseudo-TIRF setup (i.e, the laser angle was adjusted to increase penetration of the evanescent field into the sample while optimizing the signal to noise ratio). An EMCCD camera (iXon3, Andor Technologies) was used to capture images. Additional projection lenses were used depending on specific modes of imaging as described in following sections.

Flow chambers for imaging live yeast cells were constructed as follows. A coverslip (1.5, 22 mm x 22 mm) was soaked overnight in 1M NaOH, and rinsed thoroughly with nanopure water prior to imaging. It was then secured to our imaging chamber using screws and metal retainers at the edges of the cover slip. Strips of parafilm were laid across the lower coverslip and overlaid with an untreated coverslip. The parafilm was then melted on a hot plate and allowed to cool. This treatment adhered the two coverslips to each other and created a flow chamber between the upper and lower cover slips. 30µL Concanavalin A was then flowed into a dry prepared chamber and incubated for 10-20 minutes. The chamber was then washed of excess Concanavalin A, and the yeast cells introduced to the flow chamber and allowed to adhere to the surface. Excess cells were vacuumed out after a 5-10 min incubation time, and the media replaced with a sugar source and water for optimal imaging.

Growth Conditions and Media Used

To obtain lacO spacings, spindle lengths, and to assay for detachments, yeast strains were grown overnight in SDC at 26 °C, diluted into fresh SDC and grown for 4 hours at 30°C to mid-log phase before imaging at 26 °C. Imaging was done using a rapid switching triggered acquisition setup, which allowed for near simultaneous imaging in red and green channels. Cells tagged with red and green were imaged continuously with 200 ms exposure time per channel, using TIRF with a Nikon CFI Apochromat 100X 1.49 NA oil objective. For this imaging modality, the camera was fitted with a 2.5x projection lens for an effective pixel size of 64 nm per pixel.

Cells that had Cin8 under the control of the Gal promoter were grown overnight in SD containing 4% raffinose as the carbon source. Cells were diluted into SDC (with glucose as the carbon source), grown for 4 hours at 30°C until the majority of the population was in mid-log phase, and then imaged. Cells harboring the Cin8-degron were grown overnight in SDC and diluted into fresh SDC. After 2 hours of growth at 30°C, cells were washed twice, and shifted to SD containing galactose to induce Ubr1 expression, allowing for subsequent degradation of Cin8, for an additional 2 hours prior to imaging. Imaging was performed in SD containing galactose. Cells harboring the pMet-Cdc20 construct were grown overnight in SD lacking Methionine and Cysteine. They were diluted into fresh SD lacking Methionine and Cysteine for 2.5 hours, before being shifted to SD containing excess Methionine and Cysteine for 3 hours prior to imaging. Imaging was done in SD with excess of Methionine and Cysteine.

For cells harboring both the pMet-Cdc20 construct and *ipl-321* allele, the growth protocol was as described above, with cells shifted to 37°C for the last 30 minutes of growth before imaging. Imaging was done at 37°C using an objective heater and heated stage.

For cells harboring the Degron-Cin8, pMet-Cdc20 constructs and the *ipl-321* allele, the growth conditions were as follows. Cells were grown overnight in SD containing glucose, but lacking Methionine and Cysteine. Cells were diluted into SD containing glucose but lacking Methionine and Cysteine and allowed to grow for 2.5 hours at 30^{o}C. Cells were then washed twice and shifted into SD containing galactose, and an excess of Methionine and Cysteine, and allowed to grow for a further 2.5 hours at 30^{o}C. Cells were then shifted to 37^{o}C for 30 min before imaging at 37^{o}C.

To assay for spring constant, growth conditions were as described above. Imaging was done in the green channel at 30 frames per second using both an additional 1.5x and 2.5X projection lens for an effective pixel size of 42nm per pixel. Individual cells were imaged for 3 seconds or less.

For longer time-lapse movies to detect metaphase time, cells were grown overnight in SDC at 26^{o}C, diluted into fresh SDC and grown for 3 hours at 30^{o}C to mid-log phase before imaging at 30^{o}C. Imaging was done at 10 X-Y locations in the red channel at one minute intervals for 3 hours. For cells containing the Degron-Cin8 construct, cells were grown overnight at 26^{o}C, diluted into fresh SDC and grown for 2 hours. Cells were then washed twice and transferred to SD containing galactose for 2 hours prior to imaging. The imaging modality was as described. No additional projection lenses were used for longer time-lapse imaging.

To assay chromosome mis-segregation, cells were grown overnight in SDC at 26°C, then diluted into fresh SDC and grown for 2 hours at 30°C. Alpha factor was added to the culture and cells were allowed to grow for 2.5 hours before release. After release from alpha factor, cells were grown for an additional 2 hours to allow the population to enter anaphase, and then fixed and stained with DAPI prior to imaging. A previously described fixing protocol (Miller et al., 2016) designed to preserve the fluorescence of the GFP labeled lacO spots and mCherry labeled spindle pole bodies was used. Imaging was done in three channels.

Image Analysis

To analyze live yeast spindles, images of in-plane spindles were selected for analysis. All analysis of mitotic spindles was done in MATLAB (Mathworks, Natick, MA) using custom-made programs. For spindle length measurements and for calculating distance between lacO-lacI-GFP spots, a background-subtracted image was created from the raw image by filtering with a coarse-grain Gaussian filter, and then by subtracting this image from the noise-corrected image. A custom image analysis program written in MATLAB used Gaussian fitting to find the center of each spindle pole or lacO-lacI-GFP spot and then calculated the distance between the two spindle poles or lacO-lacI-GFP spots.

For metaphase time analysis, we used movies where a single cell was observed to undergo a pole duplication event, enter metaphase, and finally undergo anaphase. For each time point in the movie, spindle lengths were calculated using the algorithm described above. Metaphase time was estimated to be the interval between pole separation and anaphase onset.

For analysis of detachments and mis-segregation, individual spindles were cropped to form an image series, which were then manually scored.

To estimate the ratio in fluorescence intensity between detached diffraction-limited lacO-lacI-GFP spots and attached, separated lacO spots, we started by collecting images where a spindle with a detached chromosome and a spindle with an attached chromosome were in the same field of view. The *cin8Δ* mutant was used to maximize the chances of such pairs occurring in any given imaging chamber. We imaged both lacO spots and spindle poles and collected 7 Z-series images of 300 um width in both channels. A maximum projection was used for intensity analysis. We then estimated the background-corrected fluorescence intensity of the detached lacO spots and the averaged, background-corrected fluorescence intensity of the two lacO spots. Comparing two cells in the same field of view allowed us to control for day-to-day variations in fluorescence intensity. We also measured the average background-corrected fluorescence intensity of the spindle pole bodies. The ratio of these intensities acted as a correction factor to account for the inhomogeneity of the TIRF field, and for slight variations in spindle z-position tilt. The final formula to calculate intensity ratio was as follows. We reported the average of the ratio of all our measurements.

$$R = \left(\frac{I_{lacO,Det}}{I_{lacO,Att}} \right) \left(\frac{I_{SPB,Att}}{I_{SPB,Det}} \right) \qquad \text{(S1)}$$

Where $I_{lacO,Det}$ represented the fluorescence intensity (A.U.) of detached lacO-lacI-GFP spots, $I_{lacO,Att}$ represented the average fluorescence intensity (A.U.) of attached lacO-lacI-GFP spots, $I_{SPB,Att}$ represented the average fluorescence intensity (A.U.) of spindle poles in cells with attached lacO spots, and $I_{SPB,Det}$ represented the average fluorescence intensity (A.U.) of spindle poles in cells with detached lacO spots.

Estimation of Tension

Metaphase tension was estimated for all strains and growth conditions in the manuscript according to our previously published method for quantitatively evaluating metaphase tension in budding yeast (Chacon et al., 2014). A summary of the method is provided in Chapter 2. In this previously published work, careful methods validation was completed, and a complete explanation for the method rationale is included. For more details, please see (Chacon et al., 2014).

In the experiments used to collect the variability in distance between pairs of sister lacO-lacI-GFP tags over time, and thus to estimate the spring constant of the interkinetochore spring, cells harboring the lacO-CEN3/lacI-GFP system were grown and immobilized on cover slips as described above. 90 to 120 images were acquired for each cell using continuous single color acquisition at 30 fps. Imaging at high frame rates ensures that the observed movement of lacO-lacI-GFP spots relative to each other, as shown in a representative kymograph (Fig S1C, right) is due to thermal forces and not active forces such as those exerted by motors and microtubule dynamics. A custom MATLAB script was used for image analysis. For each frame, individual lacO

spots were localized with sub-pixel resolution using Gaussian mixture model fitting (Fig S1B), and the distance between two lacO-lacI-GFP spots was calculated. The movement of the lacO spots from one frame to the next was calculated (termed first difference) and the effect of drift was removed by fitting a line through a plot of the first differences over time for each cell. Residuals from this line were then used for the remainder of the analysis. To find the MSD for the entire population of cells for wild-type and mutant cells, the residuals for all cells were pooled, similar to previous work (Chacon et al., 2014).

Protein Purification for Western Blots

1.2 L cultures containing the Dam1-His6x and pMet-Cdc20 yeast strain, were grown at 30 °C in SD without methionine or cysteine (SD-met-cys) to log phase, and then Met and Cys were added to a final concentration of 10 mM and 2 mM respectively. Growth continued for another 3 hrs. to arrest the cells in metaphase. Cells containing the PGal-degron-Cin8 construct were grown to log phase in SD + 2% raffinose, and then galactose added to 2% at the time that Met and Cys were added, which allowed Cin8 to degrade for 3 hrs.

Cells were harvested by centrifugation and resuspended in 20 ml lysis buffer (20mM Hepes pH 7.4 / 300mM NaCl / 0.5% Triton x-100 / 5mM B-mercaptoethanol) plus protease inhibitors (1mM PMSF / 1mM AEBSF / 10uM pepstatin A / 10uM E-64 / 0.3uM aprotinin / 1mM benzamidine) and phosphatase inhibitors (10mM sodium pyrophosphate / 10mM B-glycerophosphate / 10mM NaF / 1mM Na3VO4). The cells were then lysed by liquid nitrogen freeze-grinding in a Retch RM100 mortar mill. Lysates were then centrifuge at 14000 xg, 4 °C for 1 hr. and the soluble supernatant was mixed with 1 ml of Talon metal affinity resin (Clontech

labs) for 2 hr. at 4 °C. Resin was washed extensively with lysis buffer + protease and phosphatase inhibitors, and protein was eluted from the resin by adding 1 ml of the same buffer plus 400 mM imidazole pH7, incubating for 15 min at 4 °C, and then collecting the eluate.

For the phosphatase test, the same protocol was followed except that phosphatase inhibitors were left out of all buffers, the resin was washed additionally with 50 mM Hepes / 100mM NaCl / 0.01% Brij35 + 0.1x protease inhibitors, and then protein was eluted with the same buffer + 400mM imidazole ph 7.

For the phosphatase digestion, DTT was then added to a final concentration of 2mM, 10x $MnCl_2$ (New England Biolabs) was added to 1X, and 2 ul lambda phosphatase (New England Biolabs, 400 U/ul) was added. Samples were incubated at 30 °C for 4 hrs., and then 4 °C for 24 hrs.

Western blotting

5x reducing electrophoresis sample buffer was added to samples to 1x. Samples were boiled for 6 min and added to a 12% acrylamide gel, transferred to PVDF membrane and detected with mouse monoclonal anti-6HIS antibody (clone 6-His, BioLegend), HRP-anti-mouse secondary and Supersignal West Fempto chemiluminescence reagent (ThermoFisher).

Protein Purification for Mass Spectroscopy

Cell growth, arrest, harvesting and lysis was done as described above, except that the strains contained the Dad1-TAP tag construct (gift of T. Davis) instead of the Dam1-HIS6x. In addition, the lysis buffer and phosphatase inhibitors were as described above, but the protease inhibitors

were 2mM PMSF / 2mM AEBSF / 20uM Pepstatin A / 20uM E-64 / 2mM EDTA / 0.6uM aprotinin / 20uM leupeptin / 200uM TPCK.

Soluble lysates were mixed with 200 ul of rabbit IgG-agarose resin (Sigma-Aldrich) for 1 hr. at 4° C. The resin was washed extensively with lysis buffer + protease and phosphatase inhibitors, and then washed extensively with TEV buffer (40mM Hepes pH 7.4 / 200mM NaCl / 1mM EDTA / 1mM DTT / 1mM sodium pyrophosphate / 1mM NaF / 1mM B-glycerophosphate). Resin was then mixed in 200 ul of TEV buffer with 5 ul of TEV at 2 U/ul at 4 °C for 14 hr. The eluate was collected, the resin washed with and additional 100ul of TEV buffer and both eluates combined and sent for trypsin digestion and mass spectrometry.

Mass Spectroscopy

Samples (2 µL containing 1 µg protein) for SRM analysis were subjected to injection using a manual injection loop with an analytical Eksigent HALO fused-core C18 2.7 µm, 0.3 × 100 mm connected to the Applied Biosystems 5500 iontrap fit with a turbo V electrospray source fitted for micro-flow. The samples were subjected to a gradient of 26 minutes with an Agilent 1100 micro-flow HPLC. The samples were subjected to the following gradient at a flow rate of 8 µL/minute: 0-1 minute at 5% B; 3–18 minutes a gradient to 46% B; 18–21 minutes at 95% B; and equilibrated from 21–23 minutes at 5% B, (Buffer A: Water, 0.1% formic acid; Buffer B: high-performance liquid chromatography grade acetonitrile (Fisher Scientific, Pittsburg, PA, USA), 0.1% formic acid). Transitions monitored are listed in Table S1. These were established using the instrument optimization mode with direct injection of synthetic phosphorylated and unphosphorylated peptides representing their tryptic digest of DAM1 protein. The entrance

potential (EP) was 10 V with a collision energy (CE) of 28.0 V and collision cell exit potential (CXP) of 15.0. The data were analyzed using MultiQuant™ (ABI Sciex, Framingham, MA, USA). The peak area ratio of phosphorylated/unphosphorylated DAM1 peptide was used to determine the percent of phosphorylation peptide in the reaction. Samples were run in triplicate and randomized.

Table 1: SRM Monitored Transitions

ID	Q1 Mass (Da)	Q3 Mass (Da)	Time (msec)	DP (Volts)
DAM1 (P) Y7	535.0	675.5	100.0	63.9
DAM1 (P) Y8	535.0	788.6	100.0	64.8
DAM1 (P) Y9	535.0	955.6	100.0	63.9
DAM1 Y7	495.0	675.4	100.0	64.8
DAM1 Y8	495.0	788.6	100.0	64.8
DAM1 Y9	495.0	875.4	100.0	64.8

Statistical Methods

All experiments were performed in different (independent) cells for each sample, and each experiment was replicated/performed over a minimum of 3-5 different days/experiments. Sample sizes for single image snap-shots were >100 minimum per experiment, and sample sizes for more involved experiments were as large as possible to minimize error bars.

Statistical analyses were performed by SAS 9.4 (SAS Institute, Cary, NC). All p values were 2-sided, and $p < .05$ was used to indicate statistical significance unless otherwise noted. All results for main effects and post hoc tests included in the text or figure legends were drawn from models which yielded a significant global hypothesis test.

A student's t test with pooled (equal) variances was used to evaluate the difference in spindle width between wild-type and *ase1*Δ cells.

One way analysis of variance (ANOVA) models were used to compare mean tension across strains (wild-type, *kip1*Δ, *ase1*Δ, and *cin8*Δ or degron-cin8) within a single genetic background or condition (wild type, *mad2*Δ, *ipl1-321*, or cdc20-restrictive). Similarly, a one way ANOVA was used to test for differences in tension across the three motor mutant strains with varying *cin8* modifications (i.e. *cin8*Δ, Pgal-cin8, degron-cin8*)*. Post hoc testing for pairwise comparisons between strains was conducted using the least squares means multiple comparison procedure with a Bonferroni correction ($\alpha = 0.05/n_{tests}$). To test the effect of both strain and background (e.g. wild-type vs *mad2*Δ) on tension, multivariate linear regression models were conducted with corresponding main effects. Equivalent models were used to test the effect of either strain or strain and background on metaphase time. A trend analysis with orthogonal polynomial contrast coefficients for unequally spaced factor levels was used to test for a linear or quadratic trend in increasing metaphase time with decreasing mean tension. All results are summarized as F statistics and associated p values.

Pearson chi-square analyses were used to test the associated between strain (i.e. wild type and motor mutants, or varying *Cin8* modifications) and either kinetochore detachment or mis-segregation. Cochran-Armitage tests were used to evaluate for trends across strains, with levels ordered by the strains estimated mean tension values. Statistical significance for post hoc pairwise comparisons was determined by using a Bonferroni correction. Multivariate logistic regression models with two main effects were used to test the effect of both strain and background on either detachment or missegregation. Results are summarized as either X^2 (global or main effects) or z (trend analysis) statistics and associated p values.

Appendix B : Modeling Methods

A stochastic simulation was used to investigate potential mechanisms to explain how the kinetochore detachment rate could gradually increase in response to decreasing magnitudes of centromere tension. Specifically, we tested whether a tension-dependent kinetochore phosphorylation rate could account for an increasing gradient in detachment rates with decreasing tension (Fig. 3A). This allowed us to directly ask whether a tension-dependent kinetochore phosphorylation rate could account for an increasing gradient in detachment rates with decreasing tension. Detailed simulation methods are as follows.

Simulation Initiation

The simulation was initiated by establishing a tension value ($F_{tension}$), matched to an average experimental value for both wild-type and tension mutants. This tension value remained constant throughout each simulation.

During each simulation, 500 kinetochores were independently simulated, each kinetochore with N_{sites} number of phosphorylation sites, for a duration of $t_{dur,}$ which was typically 20 minutes. At the start of the simulation, all kinetochores started in the "attached" state, and all phosphorylation sites on each kinetochore started in the "dephosphorylated" state.

Simulation Process

At each time point in the simulation, the following activities occurred (in order):

For ATTACHED kinetochores:

1) The phosphorylation rate constant is calculated based on tension, according to:

$$k_{phos} = k_{phos,0} e^{-\lambda F_{tension}} \qquad \text{(MS1)}$$

Here, the basal phosphorylation rate constant ($k_{phos,0}$) and the tension scaling factor (λ) are both free parameters, held constant for each $F_{tension}$ value in each simulation (parameter sensitivity analysis shown in Fig. S3).

2) Probability of phosphorylation (pr_{phos}) (for dephosphorylated sites) is calculated as follows:

$$pr_{phos} = 1 - e^{-k_{phos}\Delta t_{step}} \qquad \text{(MS2)}$$

Where Δt_{step} is the simulation time step size (Δt_{step}=0.01 s), and k_{phos} depends on tension, as in Eqn. MS1.

3) Probability of dephosphorylation (pr_{dephos}) (for phosphorylated sites) is calculated as follows:

$$pr_{dephos} = 1 - e^{-k_{dephos}\Delta t_{step}} \quad \text{(MS3)}$$

Where Δt_{step} is the simulation time step size (Δt_{step}=0.01 s), and k_{dephos} remained constant throughout the simulation (Table 2; k_{dephos} = 1 s^{-1}).

4) Then, each individual phosphorylation site on each kinetochore either changed its phosphorylation state, or remained unchanged, based on comparison of a uniform random number between 0 and 1 to the probabilities as calculated above. Here, if the random number was less than the calculated probability, then the phosphorylation state would switch. Otherwise, the phosphorylation state would remain unchanged.

5) Once all of the phosphorylation sites either changed states or remained unchanged, then the probability of detachment for each attached kinetochore (pr_{det}) was calculated, as follows:

$$pr_{\det} = \beta\left(\frac{N_{phos}}{N_{sites}}\right) \quad \text{(MS4)}$$

Where N_{phos} represents the number of phosphorylated sites within a kinetochore, N_{sites} represents the total number of phosphorylation sites available, and β is the detachment sensitivity factor, which scales the sensitivity of detachment with the fraction of phosphorylated sites.

6) Then, each kinetochore either detached, or remained attached, based on comparison of a uniform random number between 0 and to 1 the probability as calculated above.

Here, if the random number was less than the calculated probability, then the kinetochore would detach. Otherwise, the kinetochore would remain attached.

For DETACHED kinetochores:

1) Immediately upon kinetochore detachment, a "reattach time" ($\Delta t_{reattach}$) is calculated for that kinetochore, which represents the time that a particular kinetochore will remain detached prior to automatically attaching again. The reattach time ($\Delta t_{reattach}$, in sec.) is calculated according to:

$$\Delta t_{reattach} = (3.5 * 60) + randn * 60 \qquad \text{(MS5)}$$

This time is based on previous reports that the reattach time for kinetochores in yeast is ~3.5 minutes (Kalinina, Nandi et al. 2013). To introduce noise into this value, rand, which generates a normally distributed random number with mean = 0 and standard deviation = 1, is multiplied by 60 sec. and added to the mean experimentally reported value.

2) A detached kinetochore remains in a detached state for its entire $\Delta t_{reattach}$ time period.
3) Then, after $\Delta t_{reattach}$ has elapsed, the kinetochore automatically reattaches. At the time of reattachment, all phosphorylation sites on a kinetochore are initialized in the dephosphorylated state.

Simulation Results Reporting

After the total elapsed time is greater than or equal to t_{dur}, the stochastic simulation is complete. Then, the simulation results are reported as follows:

1) The total number of detached kinetochores is calculated, and then the detachment fraction ($frac_{Detach}$) is calculated according to:

$$frac_{Detach} = \frac{N_{kinetochores} - N_{Detached}}{N_{kinetochores}} \qquad \text{(MS6)}$$

Where $N_{kinetochores}$ represents the total number of kinetochores simulated (typically ~500), and $N_{Detached}$ represents the total number of kinetochores that were detached at the completion of the simulation.

2) In order to directly compare the simulation results to experimental results, the simulated detachment fraction (for a single kinetochore) is scaled to account for detachment events inside of cells ($frac_{Detach,obs}$), which is observed if one of two kinetochores are detached in the spindle, as follows:

$$frac_{Detach,obs} = 2(frac_{Detach}) - (frac_{Detach})^2 \qquad \text{(MS7)}$$

3) To compare experimental and simulation results, $frac_{Detach,obs}$ was recorded for each experimental tension value ($F_{tension}$), and plotted alongside experimental percent detachment results for each tension value. To quantitatively compare simulation to experiments for different simulation parameter values, a sum of squared error (SSE) was calculated for each parameter set, in which the difference between the experimental and the simulated detachment fraction was calculated and then squared for each tension, and then the values were summed across all tension values.

Table 2: Model Parameters

Symbol	Description	Value	Reference
$k_{phos,0}$	Basal Phosphorylation Rate Constant per site when $F_{tension}$= 0	1 s^{-1}	This study: matched to experimental detachment data in wild-type cells. See parameter sensitivity analysis Fig. S3D.
λ	Scaling factor that determines the influence of tension on the phosphorylation rate constant	1 pN^{-1}	Free parameter, see sensitivity analysis in Fig. S3A and Fig. 4D.
$F_{tension}$	Centromere tension	2.8, 3.3, 4 4.9 pN	Matched to experimental average tension values for wild-type and tension mutant cells
β	Sensitivity factor that scaled the fraction of phosphorylated sites with the probability of detachment	10^{-4}	This study: matched to experimental detachment data in wild-type cells. See sensitivity analysis Fig. S3B.
N_{sites}	Total number of phosphorylation Sites in the kinetochore	1-50	Simulation is insensitive to this parameter (Fig. S3); see sensitivity analysis Fig. S3C.
N_{phos}	Number of phosphorylated sites	1-50	Determined based on phosphorylation event; varies at each time step in simulation
Δt_{step}	Simulation time step size	0.01 s	N/A
k_{dephos}	Dephosphorylation rate constant	1 s^{-1}	This study: matched to experimental detachment data in wild-type cells
$\Delta t_{reattach}$	Time to reattach a detached kinetochore	210+(*rand**60) sec; where *rand* = uniformly distributed random number between 0 and 1	(Kalinina et al., 2013)
t_{dur}	Simulation duration	20 min	Metaphase time in budding yeast. (Pearson et al., 2001)

Table 3: Model Assumption Summary

Behavior	Model Assumption	Reference or Explanation
Tension-Dependent Phosphorylation Rate	Increasing tension causes an exponential decrease in phosphorylation rate of Aurora B substrates at the outer kinetochore.	(Kelly and Funabiki, 2009)
Phosphorylation dependent Kinetochore Detachments	Increasing the fraction of phospho-sites that are phosphorylated increases the probability of detachment.	(Asbury et al., 2006; Cheeseman et al., 2006; Sarangapani et al., 2013)
Tension Independent Dephosphorylation	Phosphatases at the outer kinetochore de-phosphorylate Aurora B substrates.	(Lampson and Cheeseman, 2011; Pinsky et al., 2009; Wurzenberger and Gerlich, 2011)
Reattachment	Detached kinetochores re-attach via microtubule search and capture.	(Kalinina et al., 2013)

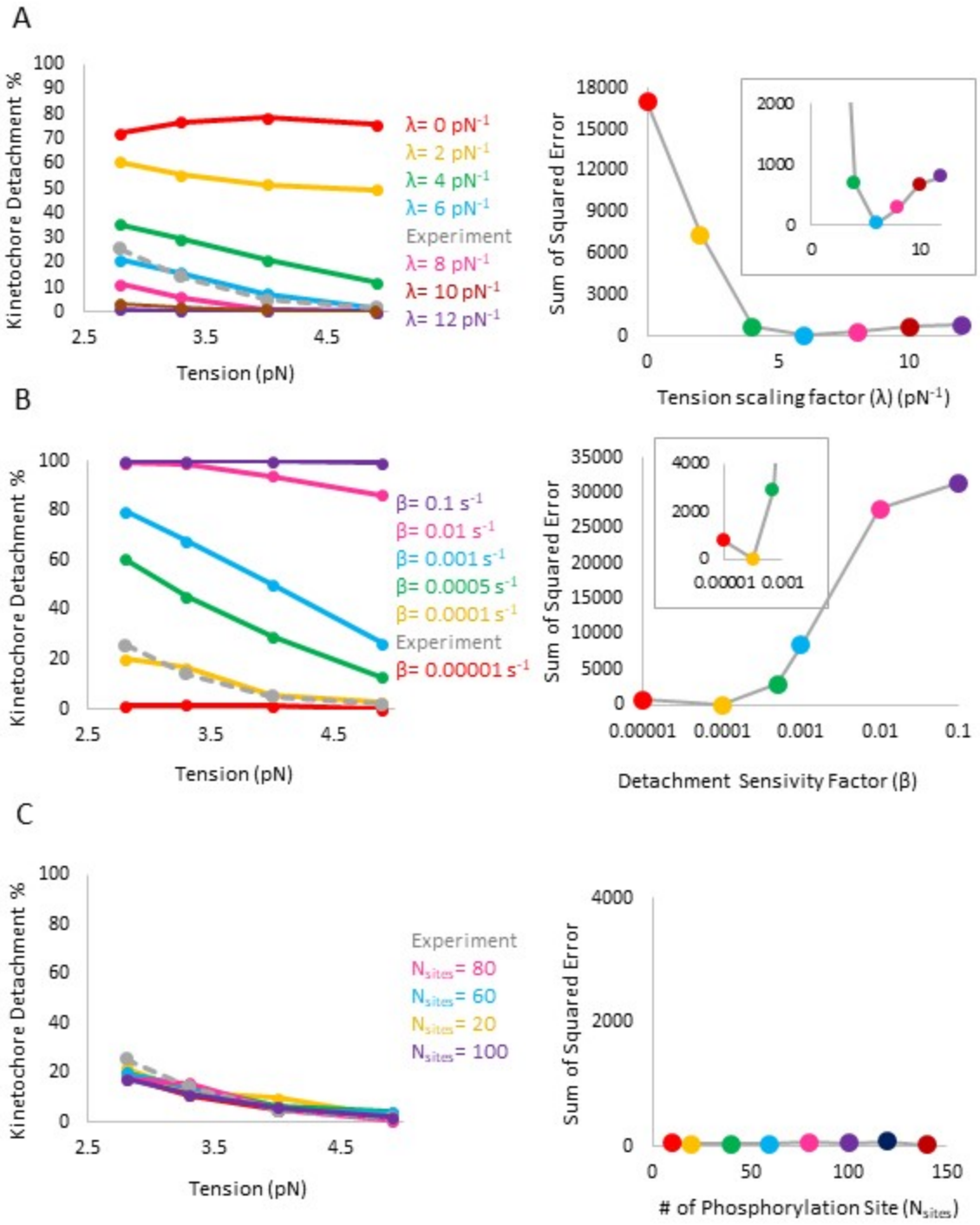

Figure 8 : Simulation parameter sensitivity analysis

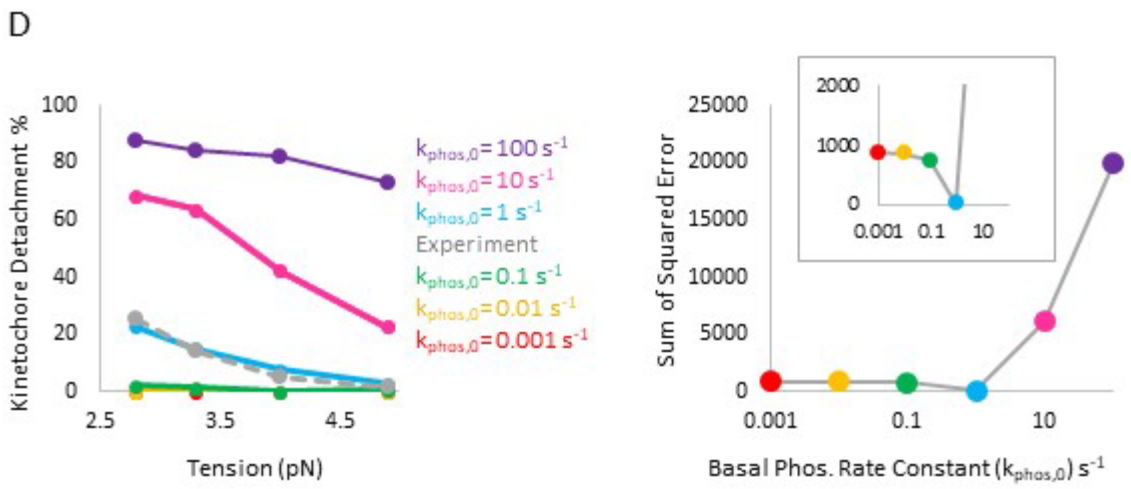

Figure 8 (contd.) : Simulation parameter sensitivity analysis

---

Figure 8: Simulation parameter sensitivity analysis. (A) Sensitivity of simulation results to the tension scaling factor (λ). Left: Detachment % vs tension for each parameter, experimental data shown in dotted grey line. Right: SSE (sum of squared errors) represents the summed error between simulation and experiment for detachment % (see simulation methods). A smaller number indicates better fit. Inset shows rescaled y-axis for clarity. (B) Sensitivity of simulation results to the detachment scaling factor (β) (note that x-axis is log to demonstrate results over 5 orders of magnitudes). Simulation results are sensitive to β for β>0.001. Left: Detachment % vs tension for each parameter, experimental data shown in dotted grey line. Right: SSE (sum of squared errors) represents the summed error between simulation and experiment for detachment % (see simulation methods). A smaller number indicates better fit. Inset shows rescaled y-axis for clarity. (C) Sensitivity of simulation results to the total number of kinetochore phosphorylation sites (N_{sites}). Simulation results are insensitive to the parameter N_{sites}, likely because results are sensitive to the fraction of phosphorylated sites, and thus are insensitive to N_{sites} within a single kinetochore. Left: Detachment % vs tension for each parameter, experimental data shown in dotted grey line. Right: SSE (sum of squared errors) represents the summed error between simulation and experiment for detachment % (see simulation methods). A smaller number indicates better fit. (D) Sensitivity of simulation results to the basal (no tension) phosphorylation rate constant ($k_{phos,0}$). Simulation results are sensitive to $k_{phos,0}$, especially for values of $k_{phos,0} > 1\ s^{-1}$. Left: Detachment % vs tension for each parameter, experimental data shown in dotted grey line. Right: SSE (sum of squared errors) represents the summed error between simulation and experiment for detachment % (see simulation methods). A smaller number indicates better fit. Inset shows rescaled y-axis for clarity.

Appendix C : Yeast Strains Used

All Strains isogenic in the W303 background unless otherwise noted. YGM005 and YGM200 are reference strains.

Table 4 : Experimental Strain List

Strain Number	Genotype	Source
YMG005	*MATa ura3-1 ade2-1 his3-11,-15 leu2-3,112 ade3Δ can1-100 trp1-1 CEN3:lacO×33(Kan) his3::GFP-lacI(HIS3) SPC110::SPC110-mCherry(hphMX)*	T. Davis; MMWY61n2a(Wargacki et al., 2010)
YMG163	*MATa CEN3:lacO×33(Kan) his3::GFP-lacI(HIS3) SPC110::SPC110-mCherry(hphMX) kip1Δ::Ura3*	This Study
YMG172 (15D background)	*MATa CEN3:lacO×33(Kan) his3::GFP-lacI(HIS3) SPC110::SPC110-mCherry(hphMX) cin8Δ::Natmx4 bar1Δ ura3 ade1 leu2 his2 trp1*	This Study
YMG191	*MATa bar1::HisG pds1::PDS1-GFP-URA3 SPC42-mCherry::HIS3*	David O Morgan DL009P (Lu et al., 2014)
YMG197	*MATa CEN3:lacO×33(Kan) his3::GFP-lacI(HIS3) SPC110::SPC110-mCherry(hphMX) ase1Δ::Natmx4*	This Study
YMG200	*MATα ura3-1 ade2-1 his3-11,-15 leu2-3,-112 can1-100 trp1-1 CEN3:lacO×33(Kan) his3::GFP-lacI(HIS3) SPC110::SPC110-mCherry(hphMX)*	This Study
YMG203	*MATa bar1::HisG pds1::PDS1-GFP-URA3 SPC42-mCherry::HIS3 cin8Δ::TRP1*	This Study
YMG208	*MATa bar1::HisG pds1::PDS1-GFP-URA3 SPC42-mCherry::HIS3 kip1Δ::TRP1*	This Study
YMG218	*MATa CEN3:lacO×33(Kan) his3::GFP-lacI(HIS3) SPC110::SPC110-mCherry(hphMX) cin8Δ::NATmx*	This Study
YMG223	*MATa ipl1-321 ade2-1 can1-100 his3-11,-15 leu2-3,-112 trp1-1 ura3-1*	Trisha Davis SFY-233-2D(Shimogawa et al., 2010)
YMG233	*MATa ipl1-321 CEN3:lacO×33(Kan) his3::GFP-lacI(HIS3) SPC110::SPC110-mCherry(hphMX)*	This Study
YMG234	*MATa ipl1-321 CEN3:lacO×33(Kan) his3::GFP-lacI(HIS3) SPC110::SPC110-mCherry(hphMX) ase1Δ::TRP1*	This Study
YMG237	*MATa ipl1-321 CEN3:lacO×33(Kan) his3::GFP-lacI(HIS3) SPC110::SPC110-mCherry(hphMX) kip1Δ::TRP1*	This Study

YMG240	*MATa CEN3:lacO×33(Kan) his3::GFP-lacI(HIS3) LacI-GFP:HIS3 SPC110::SPC110-mCherry(hphMX) mad2Δ::TRP1*	This Study
YMG242	*MATa CEN3:lacO×33(Kan), his3::GFP-lacI(HIS3) LacI-GFP:HIS3, SPC110::SPC110-mCherry(hphMX) mad2Δ::TRP1, kip1Δ::URA3*	This Study
YMG244	*MATa CEN3:lacO×33(Kan) his3::GFP-lacI(HIS3) LacI-GFP:HIS3 SPC110::SPC110-mCherry(hphMX) mad2Δ::TRP1 ase1Δ::NATmx*	This Study
YMG261	*MATa bar1::HisG pds1::PDS1-GFP-URA3 SPC42-mCherry::HIS3 ase1Δ::TRP1*	This Study
YMG264	*MATa CEN3:lacO×33(Kan) his3::GFP-lacI(HIS3) SPC110::SPC110-mCherry(hphMX) mad2Δ::URA3*	This Study
YMG281	*MATα CEN3:lacO×33(Kan) his3::GFP-lacI(HIS3) SPC110::SPC110-mCherry(hphMX) kip1Δ::TRP1*	This Study
YMG283	*MATα CEN3:lacO×33(Kan) his3::GFP-lacI(HIS3) SPC110::SPC110-mCherry(hphMX) ase1Δ::TRP1*	This Study
YMG295	*MATa CEN3:lacO×33(Kan) his3::GFP-lacI(HIS3) SPC110::SPC110-mCherry(hphMX) cin8Δ::NATmx, plasmid pGal-CIN8-TRP (p58)*	This Study
YMG302	*MATa cdc20::pMET3-CDC20::TRP1*	Tomoyuki Tanaka T4032 (Keating et al., 2009)
YMG309	*MATα ipl1-321, cdc20::pMET3-CDC20::TRP1 CEN3:lacO×33(Kan) his3::GFP-lacI(HIS3) SPC110::SPC110-mCherry(hphMX)*	This Study
YMG314	*MATa ura3-1 ade2-1 his3-11,15 leu2 trp1-1 can1-100 LYS2 GAL-UBR1 myc::HIS3, Cup1p-Nd-CIN8::URA3, SPC42-GFP::TRP*	Sue Biggins SBY3884(Kotwaliwale et al., 2007)
YMG316	*MATa CEN3:lacO×33(Kan) his3::GFP-lacI(HIS3) SPC110::SPC110-mCherry(hphMX) cdc20::pMET3-CDC20::TRP1*	This Study
YMG317	*MATa CEN3:lacO×33(Kan) his3::GFP-lacI(HIS3) SPC110::SPC110-mCherry(hphMX) GAL-UBR1myc::HIS3 Cup1p-Nd-CIN8::URA3*	This Study
YMG318	*MATα ipl1-321, CEN3:lacO×33(Kan) his3::GFP-lacI(HIS3) SPC110::SPC110-mCherry(hphMX)*	This Study
YMG320	*MATa CEN3:lacO×33(Kan) his3::GFP-lacI(HIS3) SPC110::SPC110-mCherry(hphMX) GAL-UBR1myc::HIS3, Cup1p-Nd-CIN8::URA3 mad2Δ::TRP1*	This Study

YMG322	*MATα CEN3:lacO×33(Kan) his3::GFP-lacI(HIS3) SPC110::SPC110-mCherry(hphMX) ipl1-321 GAL-UBR1myc::HIS3 Cup1p-Nd-CIN8::URA3*	This Study
YMG323	*MATa CEN3:lacO×33(Kan) his3::GFP-lacI(HIS3) SPC110::SPC110-mCherry(hphMX) cdc20::pMET3-CDC20::TRP1 kip1Δ::TRP1*	This Study
YMG325	*MATa CEN3:lacO×33(Kan) his3::GFP-lacI(HIS3) SPC110::SPC110-mCherry(hphMX) cdc20::pMET3-CDC20::TRP1 ipl1-321*	This Study
YMG326	*MATα, CEN3:lacO×33(Kan) his3::GFP-lacI(HIS3) SPC110::SPC110-mCherry(hphMX) cdc20::pMET3-CDC20::TRP1 ipl1-321*	This Study
YMG327	*MATα CEN3:lacO×33(Kan) his3::GFP-lacI(HIS3) SPC110::SPC110-mCherry(hphMX) cdc20::pMET3-CDC20::TRP1 ase1Δ::TRP1*	This Study
YMG328	*MATa CEN3:lacO×33(Kan) his3::GFP-lacI(HIS3) SPC110::SPC110-mCherry(hphMX) cdc20::pMET3-CDC20::TRP1 ase1Δ::TRP1*	This Study
YMG329	*MATα CEN3:lacO×33(Kan) his3::GFP-lacI(HIS3) SPC110::SPC110-mCherry(hphMX) cdc20::pMET3-CDC20::TRP1*	This Study
YMG332	*MATa CEN3:lacO×33(Kan) his3::GFP-lacI(HIS3) SPC110::SPC110-mCherry(hphMX) cdc20::pMET3-CDC20::TRP1 ipl1-321 GAL-UBR1myc::HIS3 Cup1p-Nd-CIN8::URA3*	This Study
YMG334	*MATa CEN3:lacO×33(Kan) his3::GFP-lacI(HIS3) SPC110::SPC110-mCherry(hphMX) cdc20::pMET3-CDC20::TRP1 GAL-UBR1myc::HIS3 Cup1p-Nd-CIN8::URA3*	This Study
YMG336	*MATα CEN3:lacO×33(Kan) his3::GFP-lacI(HIS3) SPC110::SPC110-mCherry(hphMX) kip1Δ:: cdc20::pMET3-CDC20::TRP1 ipl1-321*	This Study
YMG337	*MATa CEN3:lacO×33(Kan) his3::GFP-lacI(HIS3) SPC110::SPC110-mCherry(hphMX) ase1Δ::NATmx cdc20::pMET3-CDC20::TRP1 ipl1-321*	This Study
YMG338	*MATa CEN3:lacO×33(Kan) his3::GFP-lacI(HIS3) SPC110::SPC110-mCherry(hphMX) ipl1-321 GAL-UBR1myc::HIS3 Cup1p-Nd-CIN8::URA3*	This Study
YMG342	*MATa CEN3:lacO×33(Kan) his3::GFP-lacI(HIS3) SPC110::SPC110-mCherry(hphMX) GAL-UBR1myc::HIS3, Cup1p-Nd-CIN8::URA3 mad2Δ::TRP1*	This Study
YMG412	*MATa CEN3:lacO×33(Kan) SPC110-mCherry::hphMX DAD1-TAP-KanMx TRP1-pMET-CDC20*	This Study

YMG413	*MATα CEN3:lacO×33(Kan) SPC110-mCherry::hphMX DAD1-TAP-KanMx TRP1-pMET-CDC20*	This Study
YMG414	*MATα, CEN3:lacO×33(Kan) kip1Δ::TRP1 SPC110-mCherry::hphMX DAD1-TAP-KanMx TRP1-pMET-CDC20*	This Study
YMG415	*MATα, CEN3:lacO×33(Kan) kip1Δ::TRP1 SPC110-mCherry::hphMX DAD1-TAP-KanMx TRP1-pMET-CDC20*	This Study
YMG418	*MATα, CEN3:lacO×33(Kan) SPC110-mCherry::hphMX DAD1-TAP-KanMx ase1Δ::NATmx TRP1-pMET-CDC20*	This Study
YMG434	*MATa DAM1::6HIS-Kanmx TRP1-pMET::CDC20*	This Study
YMG442	*MATα CEN3:lacO×33(Kan) his3::GFP-lacI(HIS3) SPC110-mCherry::hphMX DAM1::6HIS-Kanmx GAL UBR1myc::HIS3, Cup1p-Nd-CIN8::URA3 TRP1::pMET-CDC20*	This Study
YMG444	*MATA CEN3:lacO×33(Kan) his3::GFP-lacI(HIS3) SPC110-mCherry::hphMX, kip1Δ::TRP1, TRP1::pMET-CDC20,DAM1-6HIS::Kanmx*	This Study
YMG446	*MATA CEN3:lacO×33(Kan) his3::GFP-lacI(HIS3) SPC110-mCherry::hphMX ase1Δ::TRP1, TRP1::pMET-CDC20 DAM1-6HIS::Kanmx*	This Study
JBY103-4A	*MAT A DAD1::TAP-KanMx*	Trisha Davis